ABSTRACT

Title of Thesis: HYDROXYAPATITE HOLLOW FIBER FOR OIL-WATER SEPARATION

Dongchang Qin, Master of Science, 2018

Thesis directed by: Professor Dr. Dongxia Liu, Department of Chemical and Biomolecular Engineering

Massive oily water produced in oil and gas industry is a catastrophe to the oil and water sources on the earth. Ceramic membrane separation is a promising approach to obtain clean water and oil fuel from oily water to mitigate this catastrophe. In this research, a low cost and biocompatible material, hydroxyapatite (HAP), is innovatively explored as bioceramic membranes for oily water separation. HAP powder was firstly synthesized by chemical precipitation and solid state exchange methods, respectively. The powder was then fabricated into membranes with various geometries such as circular pellet, dense tube, and porous hollow fiber by different methods. The preparation, property, and oil-water separation performance of HAP hollow fiber membranes were studied in details. The HAP content, particle size, viscosity of HAP suspension and sintering temperature of HAP hollow fibers all influenced the pore size, structure and oil-water separation performance of resultant HAP membranes.

HYDROXYAPATITE HOLLOW FIBER FOR OIL-WATER SEPARATION

by

Dongchang Qin

Thesis submitted to the Faculty of the Graduate School of the
University of Maryland, College Park, in partial fulfillment
of the requirements for the degree of
Master of Science
2018

Advisory Committee:
Professor Dongxia Liu, Chair
Professor Chunsheng Wang
Professor Taylor J. Woehl

©Copyright by
Dongchang Qin
2018

Dedication

This work is dedicated to my parents, Haoyun Qin and Yufeng Cheng, and parents in law, Shi Zhang and Bing Zhou, who have offered endless support and care to me during my graduate study. Without them, I cannot finish this Master's degree. I also want to give my gratitude to my wife, Simiao Zhang. She offered my endless help and care during my study.

Acknowledgements

I want to give my thanks and gratitude to my advisor Dr. Dongxia Liu for her careful guidance and instructions during my graduate study. She gave me lots of advice on how to do the research and write a paper. Without her help, I could not finish my study and research in these two years. What she said and did are good examples for me and taught me a good lesson in the past, now and in the future.

Thank you Dr. Dongxia Liu, Dr. Chunsheng Wang and Dr.Taylor J. Woehl for agreeing to serve as committee member during my graduation.

I would like to thank my labmates for their assistance during my research in Dr. Liu's lab. I want to thank Su Cheun for her help in the hydroxyapatite synthesis and characterization. I also want to thank Wei Wu for his assistance in fabrication of hollow fiber through phase inversion method and Mann Sakbodin in manufacture of tubular membrane by tape casting method. Junyan Zhang also offered me lots of help during the creation of experiment setup. Professor Yang Wang, Jingyu Fang, Emily Schulman, Richardo Morales, Wei Lu also helped me a lot during my stay in the lab. Finally, I also want to thank Dr. Jianqiang Meng and Dr. Shusen Yang from Tianjin Polytechnic University for the support in measuring pore size, Dr. Patrick Stanley for the bending strength measurement, Dr. Niti Agrawal for the viscosity measurement, and Dr. Tran Dat for assistance in the XRD measurement.

At last, I like to thank all my friends. They made my stay in the University of Maryland College Park memorable and happy.

Table of contents

Dedication ii

Acknowledgements iii

Table of contents iv

List of Tables viii

List of Figures ix

Chapter 1. Introduction ..... - 1 -

1.1 Oil-water Separation ..... - 1 -

1.2 Ceramic membrane ..... - 5 -

1.2.1 Membrane classification on morphology ..... - 5 -

1.2.2 Ceramic membrane synthesis ..... - 6 -

1.3 Hydroxyapatite ..... - 13 -

1.4 Thesis overview ..... - 16 -

Chapter 2: Hydroxyapatite powder synthesis ..... - 17 -

2.1 Introduction ..... - 17 -

2.2 Chemical Precipitation method ..... - 18 -

2.2.1 Materials ..... - 18 -

2.2.2 Experimental procedure ..... - 19 -

2.2.3 Characterization ..... - 19 -

2.2.4 Results and Discussion ..... - 21 -

2.2.5 Conclusions ..... - 25 -

2.3 Solid State method ..... - 26 -
2.3.1 Materials ..... - 26 -
2.3.2 Experimental procedure ..... - 26 -
2.3.3 Results and Discussion ..... - 26 -
2.3.5 Conclusions ..... - 30 -
Chapter 3: Hydroxyapatite membrane synthesis ..... - 31 -
3.1 Introduction ..... - 31 -
3.2 Hydroxyapatite flat membrane ..... - 32 -
3.2.1 Materials and experiment procedure ..... - 33 -
3.2.2 Results and Discussions ..... - 33 -
3.3 Hydroxyapatite tubular membrane by tape casting method ..... - 34 -
3.3.1 Materials ..... - 36 -
3.3.2 Experimental procedure ..... - 36 -
3.3.3 Results and Discussions ..... - 37 -
3.3.4 Conclusions ..... - 40 -
3.4 Hydroxyapatite hollow fiber membrane by phase inversion through single orifice .. - 41 -
3.4.1 Introduction ..... - 41 -
3.4.2 Materials ..... - 43 -
3.4.3 Experimental procedure ..... - 43 -
3.4.4 Results and Discussions ..... - 46 -
3.4.4 Conclusions ..... - 48 -
Chapter 4: Hydroxyapatite hollow fiber membrane ..... - 49 -

4.1 introduction ..... - 49 -
4.2 Experimental ..... - 51 -
4.2.1 Materials ..... - 51 -
4.2.2 Preparation of hydroxyapatite hollow-fiber membranes ..... - 51 -
4.2.3 Characterization methods ..... - 53 -
4.2.4 Water and oil water emulsion permeation test ..... - 55 -
4.3 Results and Discussion ..... - 56 -
4.3.1 Successful Recipes ..... - 56 -
4.3.2 Morphologies ..... - 58 -
4.3.3 Oil water separations ..... - 63 -
4.3.4 Regeneration of hydroxyapatite hollow fiber membrane ..... - 65 -
4.4 Conclusions ..... - 66 -
Chapter 5: Coating on hydroxyapatite membrane for the dense membrane. ..... - 67 -
5.1 Introduction ..... - 67 -
5.2 Materials ..... - 68 -
5.3 Experimental procedure ..... - 68 -
5.4 Results and Discussion ..... - 69 -
Chapter 6: Conclusions and Future work ..... - 71 -
6.1 Conclusion ..... - 71 -
6.2 Future work ..... - 72 -
6.2.1 Internal coagulant influence on the structure of hollow fiber ..... - 72 -
6.2.2 Sintering conditions on the structure of hydroxyapatite hollow fiber ..... - 72 -
6.2.3 Dense hollow fiber coated by hydrothermal growth ..... - 73 -

Reference ..... - 74 -

List of Tables

Table 1-1. Oil-water separation technologies.
Table 1-2. Comparison between conventional method and membrane technology.
Table 1-3. Advantages and disadvantages of inorganic membranes compared to polymeric membranes.
Table 1-4. Porous and Dense membranes.
Table 1-5. Summary of functions of additives in the ceramic slurry.
Table 1-6. Microstructural changes observed in solid state sintering.
Table 1-7. Property comparison of HAP and other Calcium phosphate phases.
Table 2-1. Surface area and particle size of hydroxyapatite calcined at different temperature.
Table 2-2. Surface area and particle size of solid state reaction hydroxyapatite calcined at different temperatures.
Table 3-1. Permeation results of prepared HAP (sintered at1250 ℃) and commercial ¼ inch dense Al2O3 tube.
Table 3-2. Comparison of different structure membranes.
Table 4-1. Four hydroxyapatite hollow fiber recipes with different polysulfone amounts.
Table 4-2. Four hydroxyapatite hollow fiber recipes with different N-Methyl-2-pyrrolidone amounts.
Table 4-3. Four hydroxyapatite hollow fiber recipes with different organic/inorganic ratios.
Table 4-4. Hydroxyapatite hollow fiber recipes with hydroxyapatite power calcined at different temperature
Table 4-5. Properties of hollow fiber membrane recipe 4, 20 and 30.
Table 4-6. Properties of hollow fiber membrane by variation of particle size.

List of Figures

Figure 1-1. Porous and dense membranes; symmetric and asymmetric membranes.
Figure 1-2. The three stages of heating—drying, thermolysis and sintering between the final membrane and green membrane body.
Figure 1-3. Density or shrinkage and grain size of power compact as a function of the sintering temperature. (*I*) Drying (*II*) Thermolysis (*III*) Sintering.
Figure 1-4. A two-sphere sintering model for a qualitative mechanism for grain growth in porous power compacts: (a) particles of slightly different size in contact; (b) neck growth by surface diffusion between particles; (c) grain growth.
Figure 1-5. Crystal structure and schematic illustration of stoichiometric hydroxyapatite (HAP). The blue, white, red and yellow spheres are Ca, P, O and OH.
Figure 2-1. SEM images of hydroxyapatite calcined at 600 ℃ (A), 700 ℃ (B), 800 ℃ (C), 900 ℃ (D) and 1050 ℃ (E).
Figure 2-2. XRD patterns of hydroxyapatite calcined at 600 ℃, 700 ℃, 800 ℃, 900 ℃ and 1050 ℃.
Figure 2-3. TGA of hydroxyapatite (600 ℃) without airflow.
Figure 2-4. SEM images of ssHAP-25(A), ssHAP-550(B), ssHAP-650(C), ssHAP-750(D), ssHAP-850(E), and ssHAP-900(F).
Figure 2-5. XRD patterns of hydroxyapatite calcined at 25 ℃ (ssHAP-25), 550 ℃ (ssHAP-550), 650 ℃ (ssHAP-650), 750 ℃ (ssHAP-750), 850 ℃ (ssHAP-850), 900 ℃ (ssHAP-900).
Figure 3-1. Powder pressing.
Figure 3-2. Images of Hydroxyapatite pellet. (A) pictures of pellet. Left: before calcination; Right: after calcination; (B) SEM image.
Figure 3-3. Schematic of tape casting.
Figure 3-4. Pictures of Hydroxyapatite tape membrane before and after calcination. (A) Dry membrane; (B-1) before calcination at 800 ℃; (B-2) after calcination at 800 ℃; (C-1) before calcination at 900 ℃; (C-2) after calcination at 900 ℃.
Figure 3-5. Pictures of Hydroxyapatite tube membrane. (A-1) before calcination at 800 ℃; (A-2) after calcination at 800 ℃; (B-1) before calcination at 900 ℃; (B-2) after calcination at 900 ℃; (C-1) before calcination at 1250 ℃; (C-2) after calcination at 1250 ℃.
Figure 3-6. SEM image of sintered hydroxyapatite tube membrane. (A-800 ℃) outer surface after calcination at 800 ℃; (B-900 ℃) outer surface after calcination at 900 ℃; (C-1-1250 ℃) outer surface after sintering at 1250 ℃; (C-1-1250 ℃) inner surface after sintering at 1250 ℃.
Figure 3-7. Membrane water filtration setup.
Figure 3-8. Schematic diagrams of (a) phase inversion spinning of ultrafine hollow

Figure 3-9. Pictures and SEM images of 16G and 22G hydroxyapatite hollow fiber. (A) 22G hollow fiber picture; (B) SEM image of 22G hollow fiber; (C) 16G hollow fiber picture; (D) SEM image of 16G hollow fiber.
Figure 3-10. SEM images of outer surface of 22G and 16G hydroxyapatite hollow fiber. (A) and (B): 22G; (C) and (D): 16G.
Figure 4-1. Scheme setup for the preparation of ceramic hollow fiber.
Figure 4-2. Oil water permeation test through a cross flow setup.
Figure 4-3. Cross section images of hydroxyapatite hollow fiber recipe 4, 20, 30.
Figure 4-4. SEM images hydroxyapatite hollow fiber membrane prepared with hydroxyapatite power calcined at 600 (A), 700 (B), 800(C) and 900(D)℃. 3 means the outer layer and 4 means the inner layer.
Figure 4-5. The liner relationship between bending strength and $1/\sqrt{d_g}$.
Figure 4-6. Flux(left) and Permeate concentration and rejection ratio (right) of recipe 4, 20 and 30 hydroxyapatites hollow fiber during the water permeation and oil water separation process.
Figure 4-7. Flux(left) and Permeate concentration and rejection ratio (right) of recipe A (600 ℃), B (700 ℃), C (800 ℃) and D (900 ℃) hydroxyapatites hollow fiber during the water permeation and oil water separation process.
Figure 4-8. Pore size distribution of recipe 600, 700, 800 and 900.
Figure 4-9. (Left) Flux variations of 0-time regeneration (1st time), 1 time regeneration (2nd time) and 2 times regeneration (3rd time); (Right) Permeate oil concentration and rejection ratio of 0-time regeneration (1st time), 1 time regeneration (2nd time) and 2 times regeneration (3rd time).
Figure 5-1. SEM images of the outer surface and cross-section of the first group(A-0), second group (B-1) and third group (C-2) hollow fibers.

Chapter 1. Introduction

1.1 Oil-water Separation

Massive oily water is produced in many industries, such as foods, textiles, mining, petrochemicals, oil and gas, and metal/steel industry. Oil and gas industry is the main source of the oily water and 250 million barrels oil contaminated water per day or 9-14 billion m^3 per year are produced[1]. Discharging great amount of water directly into the environment is a potential catastrophe to the water and soil source on the earth and is a big waste of valuable natural oil resources.

Strict and demanding regulations of allowable oil and grease content in the produced water have been made across different countries in the world. For example, United States Environmental Protection Agency (EPA) requests the daily maximum limit of 42 ppm for the discharged water and 29 ppm for a monthly average[2]. In China, the concentration of oil and grease in the dismissed water is just 10ppm[3]. The Australian limitation on the offshore oil and grease discharge is 30ppm[4]. With the awareness of 'greening' earth, more strict regulations or even laws about the oil content in water are expected in the future. Therefore, efficient and cost effective separation technologies are desired to produce clean water and oil fuel from massive oily water waste.

Various separation technologies have been applied for oil-water separation in past years. Table 1-1 summarizes the advantages and disadvantages of these technologies. Except for the membrane separation technology, other separation approaches can be classified into conventional methods. Although the conventional methods have been employed decades ago to

treat oily water, they are not efficient to reduce oil and grease content to satisfy the regulation requirements. Most of them are used to pretreat the oily water to remove large oil droplets or other contaminates in the water. Moreover, new pollutants arise from these processes since chemicals are often needed to the separation process. Membrane technology, however, can solve for the challenges in conventional separation methods.

Membrane separation employs a permeable or semi-permeable selective membrane barrier that permits the transport of one or more components but restricts the other of the initial mixtures, based on their physical or chemical differences between the permeating components and membrane. In oily water separation, no chemical additive is required in the membrane separation process since it is a pressure driven process and the separation depends on the pore size of the membranes. According to materials used, membrane could be classified into inorganic and organic membrane. Polymer membrane is widely and commercially utilized due to its wide variability of barrier structure and properties, and robustness to control pore size, size distribution, density and shape, but the polymer membrane separation efficiency is affected by polar solvents, chlorinated solvents and high oil fraction[1]. The reusability of polymeric membranes has been a challenge due to difficult regeneration capability by simple method such as calcination. Inorganic membrane materials often include ceramics, metallic, carbon, glass and zeolite. In oily water separation, the inorganic membranes exhibit higher mechanical and chemical stability, reliability and stability, lower overall life cycle cost[5]. Table 1-3 shows the characteristics of inorganic membranes when compared to organic membranes in oil-water separation.

Table 1-1. Oil-water separation technologies[6].

Method	Advantages	Disadvantages

Multimedia filtration	Efficient retention of solid particles and oil droplets larger than 10 micrometers	Not effective in retention of small oil droplets and dissolved contaminants
Solvent extraction	Efficient, fast	High cost, not sustainable, no heavy metal removal
Centrifugation	Easy, robust, sustainable, no additives	High energy demand, minimal droplet size is 2 micrometers
Induced gas flotation (no flocculants)	Easy to apply, energy-efficient process	Removes oil droplets larger than 25 micrometers, WOR extremely high
UV irradiation	No waste stream, fast and effective, no chemicals	Expensive equipment, fouling of UV lamps, unable to treat heavy metals
Chemical precipitation followed by gravity settling	Easy to process, efficient removal of heavy metals, flexible	High cost, high energy demand, low efficiency for dissolved components, secondary purification for chemicals/water is needed
Adsorption	Short treatment process, suitable for cold regions, compact packed bed modules, cheap, efficient	High retention time, following treatment required, heavy metals not removed
Air stripping	Very fast, efficient, no chemicals, proven technology	Creates a new waste stream, costly, impractical for small areas, heavy metals not removed
Pyrolysis	Large treatment capacity, fast and effective	High CapEx and OpEx
Incineration	Rapid, complete removal of hydrocarbons in oily sludge	High CapEx, separate process to remove ash is required, applicable to high oil concentrations
Oxidation	Rapid and simple, complete decomposition of hydrocarbons	Large number of chemicals, high cost, disposal of toxic waste
Biological treatment	Less cost and large treatment capacity	Very slow process, large mass of sludge produced, high footstep
UF membrane treatment	High efficient, cost-effective, no added chemicals, small footprint, low CapEx and OpEx	Low retention of heavy metals and dissolved organics

Table 1-2. Comparison between conventional method and membrane technology[1].

Conventional method	**Membrane Technology**

Only suitable for pre-treatment of wastewater for in situ reuse	Less complex & preferable for medium and large offshore platforms
Large amount of energy and chemical additives required, economically unfit and lower size molecules difficult to settle down	Theoretically, no chemical additives, thermal inputs, or regeneration of spent media
Very slow and complicated process and required more area	Simple operational mechanism
Often involved spent chemical that leads to chemical pollutants	High reusability properties that allows recycling
Limited room for improvement since most of them are rigid and exacting	Robust, allows rooms for further improvement and integration in development of better performing treatment technology

Table 1-3. Advantages and disadvantages of inorganic membranes compared to polymeric membranes[7].

Pros	Cons
Long term stability at high temperatures	High capital cost
Resistance to hard environments (chemical degradation, pH, etc.)	Embrittlement phenomenon
Resistance to high pressure drop	Low membrane surface per module volume
Inertness to microbiological degradation	Difficulty of achieving high selectivity in large scale microporous membranes
Easy cleaning after fouling	Generally low permeability of the highly hydrogen selective (dense) membranes at medium temperatures
Ease catalytic activation	Difficult in membrane module sealing at high temperature

1.2 Ceramic membrane

Ceramic membranes are one type of inorganic membranes in oily water separation. Ceramics are defined as non-metallic solids hardened by heat and subsequent cooling according to the *Ceramic Tile Institute of America*[8]. Generally, ceramic materials are composed of a metal (e.g. aluminum, zirconium, titanium, calcium, iron) and a non-metal element (like oxygen, nitrogen, phosphate or carbon), such as aluminum oxide and zinc oxide. Below, we introduce methods for synthesis of ceramic membranes.

1.2.1 Membrane classification on morphology

When classified per their morphologies, membranes could be porous or dense and symmetric or asymmetric. Porous membrane has a porous separation layer and the separation efficiency (i.e. flux and selectivity) is mainly determined by the pore sizes rather than the materials. The intrinsic properties of membrane materials of nonporous or dense membranes account for the mobility of molecules through the membrane. Porous membranes are classified into microporous (dp< 2 nm), mesoporous (2 nm <dp < 50nm) and macroporous (dp>50nm) membranes based on pore sizes by IUPAC[9]. Transportation mechanisms and applications of porous and dense membranes are shown in Table 1-4. Symmetric (isotropic) membranes have a uniform structure throughout the entire membrane and asymmetric (anisotropic) membranes show a non-uniform structure with a selective dense or porous skin layer and a porous support. The flux and selective in the asymmetric membranes are mainly determined by the skin layer and the support layer provides mechanical strength and stability. In the symmetric membrane, mass transfer depends on the total thickness of the membrane and membrane thickness decreasing leads to higher permeation rate and lower mechanical strength. Symmetric membranes are widely used in dialysis, electro-dialysis and microfiltration[10].

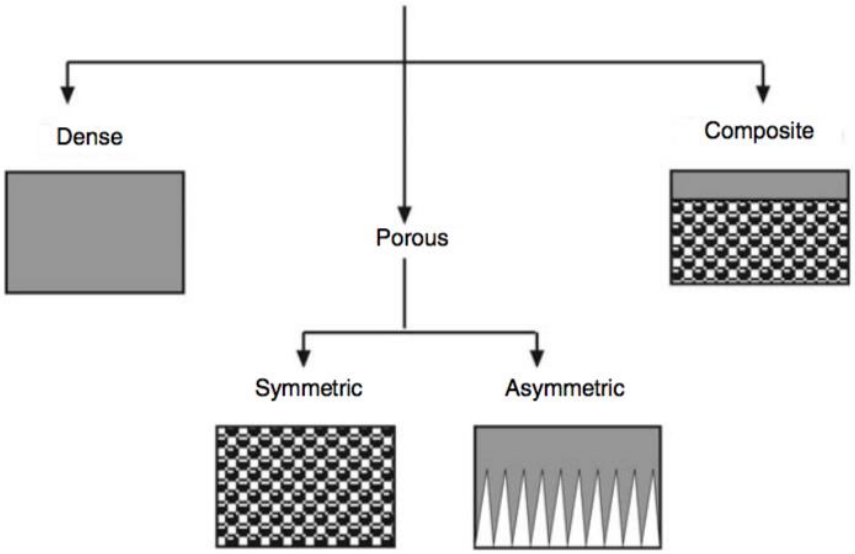

Figure 1-1. Porous and dense membranes; symmetric and asymmetric membranes[11].

Table 1-4. Porous and Dense membranes.

Type	Pore size (nm)	Mechanism	Applications
Macroporous	>50	Sieving	UF, MF
Mesoporous	2-50	Knudsen diffusion	UF, NF, Gas Separation
Microporous	<2	Microspore diffusion	Gas Separation
Dense	-	Diffusion	Gas separation, Reaction

1.2.2 Ceramic membrane synthesis

Many methods can be used to make ceramic membranes, including slip casting, tape casting, extrusion, pressing, pyrolysis, sintering of ceramic slurry, sol-gel synthesis, dip-coating, hydrothermal treatment, chemical vapor deposition, etc[12]. Generally, the ceramic membrane contains the active layer supported on a porous support substrate. The membrane support can be made by three mains steps: (a) mixing the ceramic powder, solvent and additives to form a

ceramic slurry; (b) shaping the slurry into designed geometries by extrusion, tape casting, or slip casting methods; and (c) evaporating solvents and sintering the membranes.

1.2.2.1 Ceramic slurry preparation

The initial ceramic slurry is prepared by homogeneously mixing ceramic power with solvent and other chemical additives. Many factors in the ceramic slurry influence the membrane properties. Monodispersed ceramic power is preferred, since ceramic particles with a wide range of size distribution will lead to large pore size distribution in the synthesized ceramic membranes. The small particle sizes often reduce the pore size and flux but enhance the mechanical strength of the final sintered membranes. There are some empirical equations that correlate the tensile strength of a support σ_t, pore size d_p and grain size d_g. The tensile strength σ_t is proportional to $1/\sqrt{d_g}$. Large grain size results in small tensile strength[13]. The ratio of pore size d_p and grain size d_g is between 2:5 and 2:3[14]. However, this ratio is significantly affected by the grain shape. Higher particle to total slurry ratio (packing density) strengthens the membrane and declines the membrane permeability. The highest packing density 0.74 could be achieved by ordered packing of uniform spherical grains in parallel hexagonal arrangement (Barlow packing) if only uniform grains are considered[15]. This highest packing density or even higher packing density could be reached by addition of small size grains into the suspension. In the slurry, ceramic grains should be equally and separately dispersed in the solvent. Therefore, essential chemical additives like dispersant and binder are needed to prevent the agglomeration of grains and cracks in the green membranes. Table 1-5 shows the common additives and their corresponding functions. More detailed information will be introduced in chapter 3.

Table 1-5. Summary of functions of additives in the ceramic slurry[12].

Additive	Function

Solvent	Suspends the ceramic powder and dissolves additives and binders that form the initial slurry
Deflocculant/dispersant	Increases the electrostatic repulsion or the steric hindrance of grains in aqueous and non-aqueous suspensions, respectively, and prevents aggregation
Binder	Maintains green body features and prevents cracking at drying and sintering
Plasticizer	Penetrates the binder to structurally expand it and improve its distribution in the slurry
Antifoam	Prevents or destroys foam
Lubricant	Helps in releasing the green body from its mold
Chelating agent	Inactivate undesirable ions
Fungicide/bactericide	Stabilizes against degradation with ageing

When particles are homogeneously dispersed in the slurry with adjustable amounts of additives, the slurry is ready for shaping after an additional degassing process to remove potential air bubbles by vacuum pump and a gentle stirring. The membrane shape determines the method used. In general, plate, tube, hollow fibers and honeycomb monoliths are prepared by dry pressing, extrusion or slip/tape casting. More information about how to prepare desired shape membrane will be discussed in chapter 3.

1.2.2.2 Sintering

The last step to finalize the properties of the membrane is a heating process containing dry (pre-sintering), thermolysis and sintering to remove the solvent and additives and harden the membranes. In the dry process, all the solvent evaporates at room temperature or lower than 200 ^{o}C, but the chemical additives still exist and promote to sustain the membrane morphology. Concurrently, particles come to contact with each other directly. The dry step is the only reversible step among the heating process and addition of solvent will recovery the original green membrane condition. Thermolysis removes the chemical additives such as binders and

plasticizers at high temperature, which results in the decomposition of chemical additives into volatile organic compounds and carbon residues. Removal of the chemical additives could lead to the pore, which is expected for preparation of porous membranes. However, incomplete or un appropriate removal of additives defects the membrane and then affects the membrane performance. One important factor for themolysis is the binder. Higher binder concentration will lead to the formation of non-volatile compounds, which must be avoided during the manufacture process. The ratio of binder to particle volume should be below 0.08-0.15 to prevent the formation of non-volatile compounds[16]. Thermoplastic binders can result in pore formation and thermoset binders may bring cracks in the thermolysis process. After the optimization of binder (kind and amount) and thermolysis process (condition, heating rate and duration time), green membrane should keep its structure without cracks, distortion, deformation or expanded pores. Figure 1-3 shows the density and grain size variation with each heating step. In the drying process, grain size and density do not change. In the thermolysis, rapid densification with little

grain growth occurs, but rapid gran growth with little densification happens in the final sintering stage.

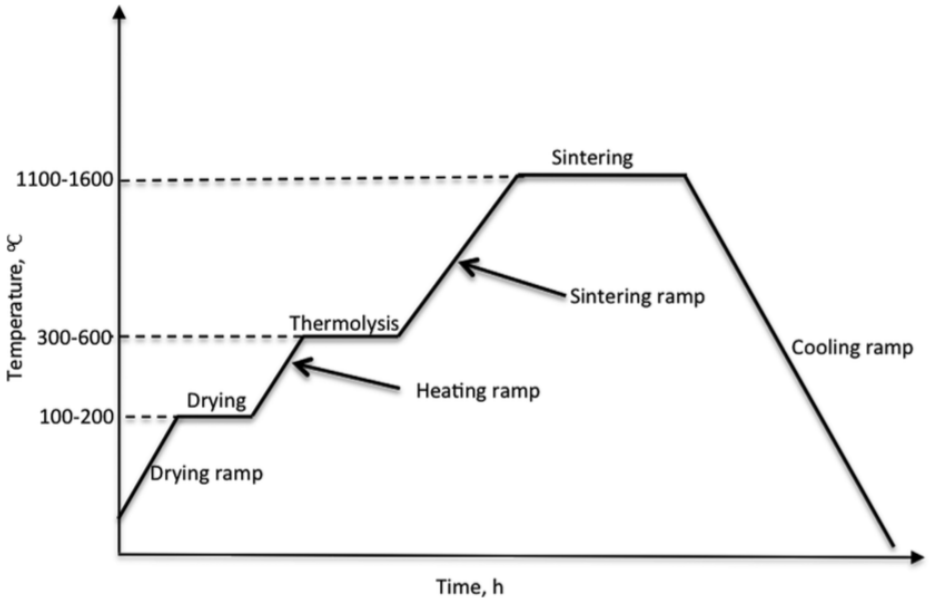

Figure 1-2. The three stages of heating—drying, thermolysis and sintering between the final membrane and green membrane body.

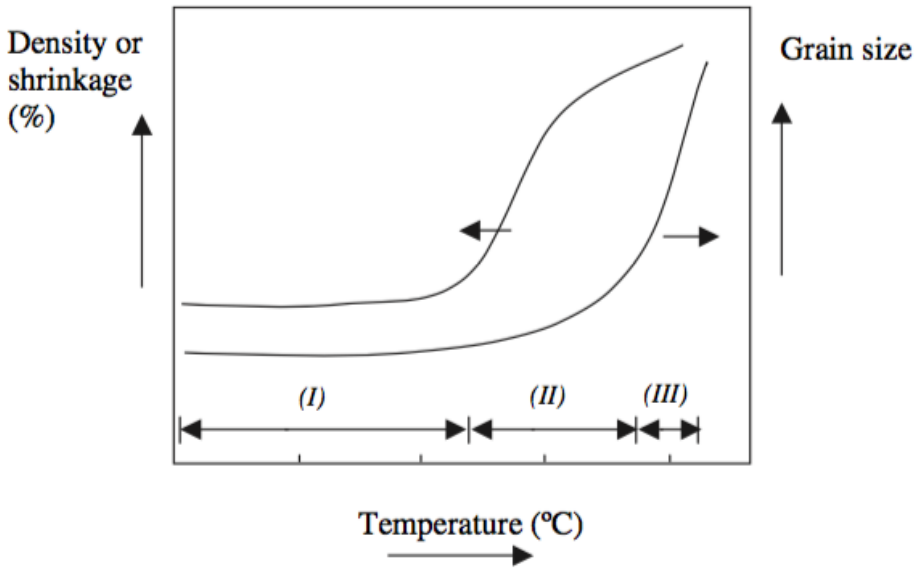

Figure 1-3. Density or shrinkage and grain size of power compact as a function of the sintering temperature[17]. (*I*) Drying (*II*) Thermolysis (*III*) Sintering.

Sintering is the finishing and most important stage in the heating treatment of membrane. Sintering is a process that consolidate the materials by heating. Sintering types contain solid-state, liquid phase, viscous sintering and verification. Solid state sintering, especially solid state pressure less conventional sintering is widely applied in the ceramic membrane heating treatment process. The sintering temperature ranges between 0.5~0.9 of the melting point of the ceramic particles[18]. Sintering process could be kinetically divided into initial, intermediate and final stages.

The characteristics of each stage are shown in Table1-6 and Figure 1-4. During the heating process, external energy liberates atoms within the grain. As shown in Figure 1-4, a solid neck arises between two contact grains due to the mobility within the grain. Diffusion between the surface and inner vacancies promotes the formation of the solid neck and grain boundary diffusion supports appearance of channel like pores. These channel like pores collapse to separated voids, which are excluded during the final sinter stages.

The sintering process is very complicate and two factors should be remarked, grain growth and pore evolution. Grain growth describes the grain size increasing process at sufficiently high temperature. The driving force of grain growth is the decrease in grain boundary energy due to the decrease in the surface area. The difference in the grain boundary energy promotes the grain growth and grain boundary energy of all grains are same in the stable structure. The shape of the grain tends to turn into hexagon, since the grain boundaries are straight when the edge number equals to 6. Grains with edge number larger than 6 tend to grow and grains with edge number smaller than 6 tend to shrink. The grain growth leads to the pore evolution. A pore is circled around by N number of grains and N is called the pore coordination number. In the pore evolution process, the surface of the pore moves to the center of curvature.

Pore with $N < 6$ will shrink while pore with $N > 6$ will expend. When N equals to 6, the pore is metastable and pore size might decrease or increase. For a dense membrane synthesis, the pore with $N < 6$ is preferable. Another common term to describe the sintering is coarsening, which contains both the grain growth and pore evolution process. Large number of factors influence the sintering. Even tiny factors in the synthesis process might affect the sintering. For example, higher sintering temperature promotes the densification of the membranes with superior mechanical strength, low porosity and flux. Smaller grain size leads to denser membranes with higher mechanical strength, as shown in Figure 1-3.

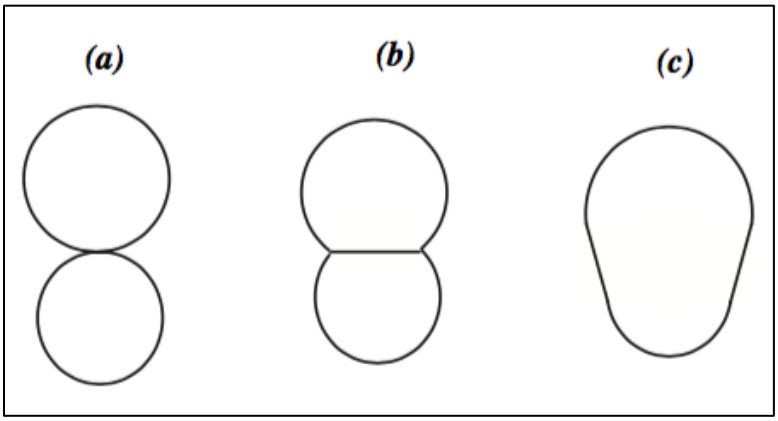

Figure 1-4. A two sphere sintering model for a qualitative mechanism for grain growth in porous power compacts: (a) particles of slightly different size in contact; (b) neck growth by surface diffusion between particles; (c) grain growth[12].

Table 1-6. Microstructural changes observed in solid state sintering[17].

Additive	Function
Initial: rapid interparticle neck growth by diffusion, vapor transport, plastic flow or viscous flow.	• Surface smoothing of particles • Grain boundaries form, neck growth • Rounding of interconnected, open pores • Porosity decreases <12% and linear shrinkage of 3-5% • Density up to 0.65 of the theoretical

Intermediate: begins when the pores have reached their equilibrium shapes as dictated by the surface and interfacial tensions. It normally covers the major part of the sintering process. Shrinkage is induced by grain growth and a change in the pore geometry. More than one mass transport mechanism may be contributing significantly to the changes in microstructure.	• Equilibrium pore shape with continuous porosity • Shrinkage of open pores intersecting grain boundaries • Mean porosity decreases significantly • Slow grain growth (differential pore shrinkage, grain growth in heterogeneous material) • Density range from 0.65-0.90 of the theoretical
Final: the pores are assumed to shrink continuously and may disappear altogether	• Equilibrium pore shape with isolated porosity • Closed pores intersect grain boundaries • Pores shrink to a limited size or disappear • Pores larger than grains shrink relatively slowly • Grains of much larger size appear rapidly • Pores within larger grains shrink relatively slowly

Ceramic membrane has showed good separation efficiency for oil water separation. A rejection of up to 99% of oil by Al_2O_3, TiO_2/Al_2O_3 and TiO_2 membranes was reported by *Ebrahimi* et al[19]. Other ceramic materials that have been tested for oily water separation are SiO_2 and ZrO_2.

1.3 Hydroxyapatite

Hydroxyapatite (HAP) is the major mineral component of vertebrate hard tissues like teeth and bones. It is reported that 70% of natural bones are monocrystalline HAP with length of 20-80 nm long and width of 2-5 nm[20]. HAP is in non-stoichiometric form, which contains trace amount of impurities, such as carbonate, sodium, magnesium, and its structure varies with the

tissue types[21]. As a biomaterial, hydroxyapatite is widely used in bone tissue regeneration(osteogenesis), implanting materials coating and drug delivery [22].

In one unit cell of crystalline hydroxyapatite, four Ca (M1) atoms are encircled by nine oxygen atoms from phosphate group and the other ten Ca atom (M2) are surrounded by six oxygen atoms. Two M1 Ca atoms and four M2 atoms enfold one hydroxyl group to form a hydroxyl channel[23]. The crystal structure of hydroxyapatite is hexagonal crystal system $P6_3/m$ with two main crystal planes: *a* plane and *c* plane (Figure 1-5). The cell parameters are a=b=9.418 Å and c = 6.884 Å[24].

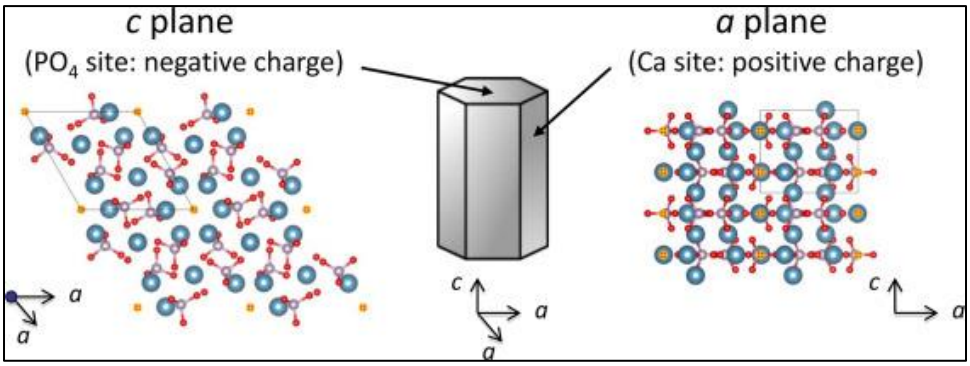

Figure 1-5. Crystal structure and schematic illustration of stoichiometric hydroxyapatite (HAP). The blue, white, red and yellow spheres are Ca, P, O and OH[25].

Hydroxyapatite is the most stable derivative of calcium phosphate salt within the pH range of 4-14 at 25 °C, which is the foundation of the hydroxyapatite synthesis methods. Table 1-7 shows the property comparison of HAP and other common calcium phosphate phases. Hydroxyapatite has a low solubility in water and stabilizes in a wide range of pH. Different kinds of hydroxyapatite are convertible. For example, hydroxyapatites dehydrate to tricalcium phosphate at high temperature[26] and HAP was synthesized by hydrolysis of dicalcium phosphate[27].

Table 1-7. Property comparison of HAP and other Calcium phosphate phases[28, 29].

Name	Hydroxyapatite	α-Tricalcium phosphate	β-Tricalcium phosphate	Dicaclcium phosphate	Monocaclim phosphate
Symbols	(HA) and (HAP)	(α-TCP)	(β- TCP)	(DCP)	(MCP)
Formula	$Ca_{10}(PO_4)_6(OH)_2$	$Ca_3(PO4)_2$	$Ca_3(PO4)_2$	$CaHPO_4$	$Ca(HPO_4)_2$
Molar mass (g/mol)	502.31	310.18	310.18	136.06	234.05
Melting point (^oC)	1614	1391	1391	1670	109
Molar ratio (Ca/P)	1.67	1.5	1.5	1.0	0.5
Solubility in water 25 ^oC (g/L)	0.0003	0.0025	0.0005	0.0048	17
Space group	Pseudohexagonal $P6_3/m$	Monoclinic $P2_1/a$	Rhombohedral R3cH	Triclinic P^1	Triclinic P^1

Except for its applications in biomedical field, hydroxyapatite is widely applied in non-medical applications. As a catalyst, hydroxyapatite contains both acid and base active sites in a single crystal and could be applied in ethanol to butanol reaction through Guerbet mechanism[30], Friedel-Crafts reaction[31], and hydrogen transfer[32] etc. Hydroxyapatite exhibit good performance in water treatment and remediation of heavy metal contaminated soils[33, 34]. Hydroxyapatite could also work as ion conductors[35], gas sensors[36] and column chromatography materials for proteins and nucleic acids separation[37]. In this work, hydroxyapatite as a ceramic material were manufactured into oil-water separation membranes and their property and separation performance were studied.

1.4 Thesis overview

The objectives of this thesis are to prepare different morphologies hydroxyapatite membrane and apply hydroxyapatite hollow fiber membrane in oil water separation. The synthesis of hydroxyapatite by chemical precipitation and solid state method were discussed in chapter 2. Chapter 3 mainly focuses on the three-different shape hydroxyapatite membrane synthesis, including the disk membrane by cold pressing method, flat or tubular membrane by tape casting process and hollow fiber membrane through a single orifice spinneret by combination of phase inversion method and spinning method. Chapter 4 discusses the phase inversion process that hydroxyapatite hollow fiber membrane was prepared through a coaxial spinneret and the application of the hollow fiber membrane in oil water separation. Chapter 5 provides a hydrothermal growth method to prepare a dense layer on porous HAP hollow fiber membrane. Chapter 6 summarized the results in this thesis work and proposed future work.

Chapter 2: Hydroxyapatite powder synthesis

2.1 Introduction

To prepare hydroxyapatite ceramic membrane, hydroxyapatite power, as the starting material for membrane formation, is needed. Different methods can be used to fabricate HAP membranes with different geometry, and the HAP powder with different surface areas that is determined by the particle size are in need. HAP powder can be prepared by various methodologies, including solid state method synthesis[38-40], mechano-chemical [41-43], chemical precipitation[30, 44-48], sol-gel[49-51], emulsion[52-54], hydrolysis[27, 55, 56], hydrothermal growth[57-59], microwave-assisted [60-62]. Among all these methods, Chemical precipitation is well practiced in literature which usually produces small particle sizes and thus high surface area. The solid-state synthesis can make large particles with low surface area. In our study, we employed these two methods to purposely make the HAP powder with various surface areas. As discussed in chapter 3, the surface area is an important factor that determines the procedure to use and membrane quality produced in each membrane synthesis process.

In the chemical precipitation process, the calcium reagents and phosphate reagents are mixed together first in the aqueous conditions and then the mixture is stirred under specific temperature and pH conditions. The reason for the formation of hydroxyapatite is that it is the most stable and less soluble calcium phosphate apatite in aqueous condition at 25 ^{o}C when pH equals 4.2.[63, 64] Varying synthesis conditions achieve diverse crystallinity, morphology and Ca/P ratio hydroxyapatite. Properties of hydroxyapatite will determine the quality of ceramic membrane, and this ceramic

membrane is expected to have high mechanical strength. The stoichiometric ratio of Ca/P (1.67) corresponds to the hydroxyapatite materials with largest value of strength.[65] One specific chemical precipitation method was proposed that when the solution pH is 10.5 and the mixture is mixed with stirring under 80 ^{o}C for 24hrs, the synthesized hydroxyapatite powder is stoichiometric and uniform with rod-like structure.[30] This method would be used to make the desired hydroxyapatite samples.

Solid state synthesis method is not widely studied because the small diffusion of ions in the synthesis process leads to impurities in the HAP, even though solid state method is a common choice for industry to manufacture other powders due to its simplicity. Like chemical precipitation, in the solid-state method, calcium and phosphate precursors are mixed together, then milled and calcined at high temperature to form well-crystallized structure. A novel refined solid state method was applied to synthesize crystalline hydroxyapatite and discuss effect of calcining temperature[40]. During this method, solid mixture will turn into paste mixture, which could improve the diffusion of ions. The results show that pure hydroxyapatite is formed when the calcination temperature is lower than 700 ^{o}C. This method is also used in this work to synthesize small surface area hydroxyapatite powder.

2.2 Chemical Precipitation method

2.2.1 Materials

Calcium Nitrate Tetrahydrate (ACS, 99.0-103.0%) and Ammonium hydrogen phosphate (ACS, 98.0% min) were purchased from Alfa Aesar through VWR. Ammonium Hydroxide (ACS, 28-30%) were purchased from BDH CHEMICALS. ISOPROPYL ALCOHOL (99%, reagent ACS USP/NF Grade) was bought from

PHARMCO-AAPER. All chemicals were used as received without any treatment and Deionized (DI) water was used in all purpose.

2.2.2 Experimental procedure

0.6 M calcium nitrate tetrahydrate and 0.4 M ammonium hydrogen phosphate were slowly mixed together and the pH of the mixture was adjusted to 10.5 by ammonia hydroxide. The solution was stirred at 80 ^{o}C for 24hrs and then the precipitate was filtered and washed. Finally, the sample were dried and then calcined at 600 ^{o}C for 6hrs with air flow. The hydroxyapatite powder was also calcined at 700 ^{o}C, 800 ^{o}C, 900 ^{o}C and 1050 ^{o}C by 2 ^{o}C/min for 4hrs without airflow to discuss the calcination effect on the hydroxyapatite properties.

2.2.3 Characterizations

Powder X-ray Diffraction of the synthesized hydroxyapatite were measured by a Bruker D8 Advance Lynx Powder Diffractometer (LynxEye PSD detector, sealed tube, Cu Kα radiation with Ni β-filter). An Autosorb-iQ analyzer (Quantachrome Instruments) measures N_2 adsorption-desorption isotherms, from which the surface area of the particles was calculated. All the samples are degassed at 1mmHg and 245 ^{o}C for 8 hours before measurements. The specific surface area was calculated by the Brunauer, Emmett and Teller (BET) method. Dynamic Light Scattering (DLS) was used to measure the particle size of the materials. The measurement was conducted on a Photocor-FC light scattering instrument with a 5-mW laser light source at 633 nm. The temperature was 25 ^{o}C and the scattering angle was 90 ^{o}C. The particle sizes could be calculated by the autocorrelation function by the Photocor software and a logarithmic correlator was used to measure the autocorrelation function. For the particle size measurement, since

hydroxyapatite particle is unstable in the water, approximately 0.1 g particles were dissolved in isopropanol and sonicated by Bransonic 1510R-DTH for 30 mins and then diluted 100 times by isopropanol for another 30-min sonication. The morphologies of the hydroxyapatite were recorded by scanning electron microscopy (SEM) on a Hitachi SU-70 electron microscope. The stability of the samples was measured by Thermogravimetric analyzer (SHIMADZU TGA-50) at 5 ^{o}C/min without airflow.

2.2.4 Results and Discussion

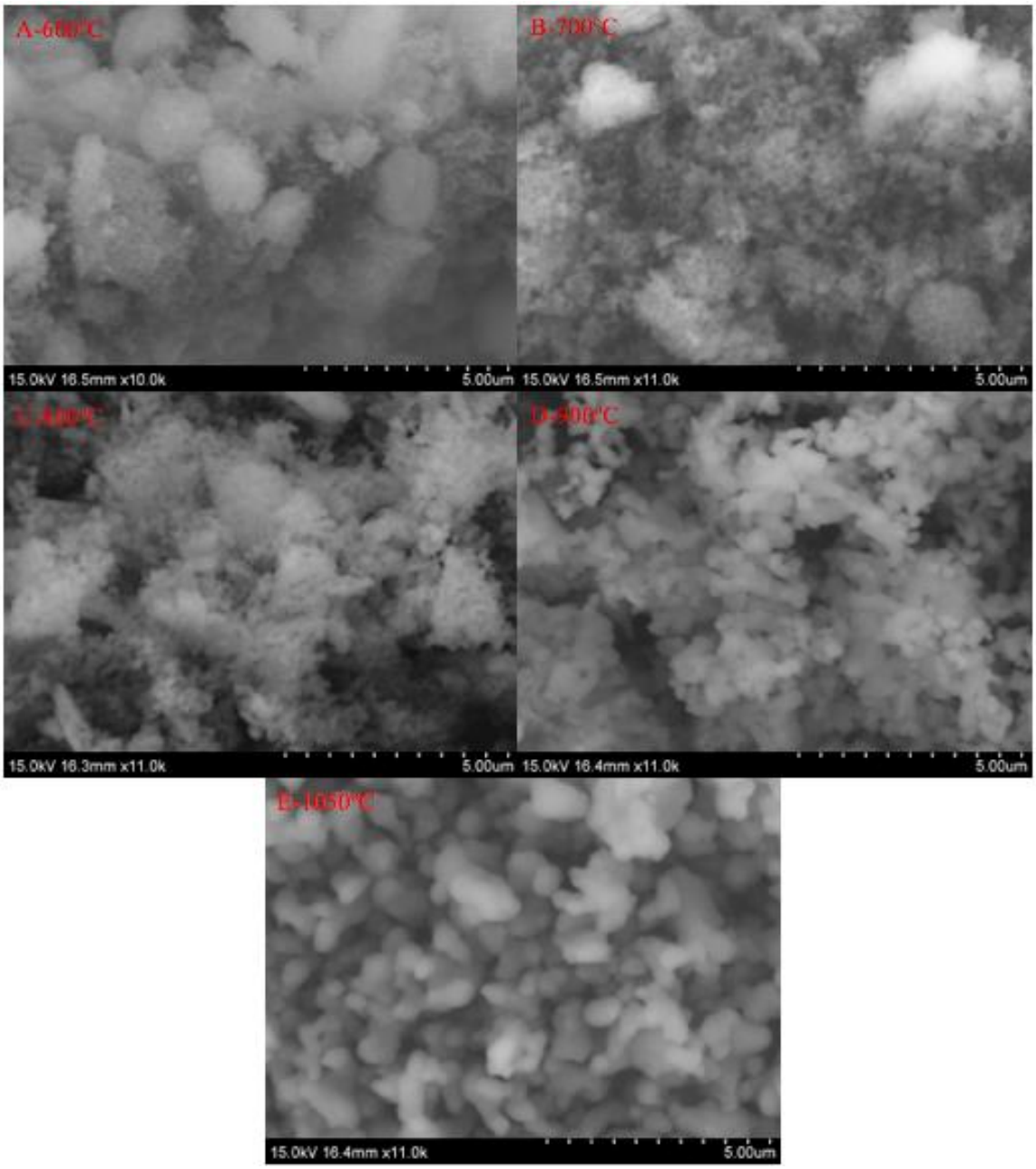

Figure 2-1. SEM images of hydroxyapatite calcined at 600°C (A), 700°C (B), 800°C (C), 900°C (D) and 1050°C (E).

Table 2-1 shows the specific area and particle size of hydroxyapatite power calcined at different temperature. Higher calcination temperature increased the particle size from 211.17 nm to 525.86 nm and the surface area decreased from 34.903 m^2/g to

7.474 m^2/g correspondingly due to the sintering effect. The variation of surface area is consistent with the change in particle size.

The SEM images indicate the same effect. From 600°C to 1050°C, the particle size increased (Figure 2-1). When the temperatures were low (600, 700 and 800 °C), the particles agglomerated together and the morphologies were needle or rod-like. Figure 2-1 A, B and C show that the particle size of hydroxyapatite treated by 600 and 700 °C was smaller than 200 nm and hydroxyapatite treated by 800 °C was approximately 200 nm. Particle sizes indicated by SEM were much smaller than DLS, where the particles agglomerate in the isopropanol solution. SEM images also reveal some agglomeration of particles. When treated at a higher temperature (900 and 1050 °C), particles are dispersed (Figure 2-1 D and E), with rod-like shape and larger particle size. Both particle sizes for 900 and 1050 °C (Figure 2-1 D and E) is around 500 nm. This size is approximately the same as the one measured by DLS (525.86 and 534.13), which means that those particles disperse separately in the isopropanol solution.

Table 2-1. Surface area and particle size of hydroxyapatite calcined at different temperature.

Calcination Temperature(°C)	Surface area(m^2/g)	Particle size/radius(nm)
600	34.903	211.17
700	18.090	231.52
800	10.786	389.68
900	7.474	525.86
1050	1.536	534.13

X-ray diffraction patterns of five different calcination temperature samples are shown in Figure 2-2. All samples have clear characteristic peaks of crystalline

hydroxyapatite[57]. With increase of calcination temperature, peaks vary from broad to sharp, which indicates the enhancement of crystallinity. When the calcination temperature is lower than 700 ^{o}C, only hydroxyapatite crystalline peaks emerge. When calcination temperature is higher than 700 ^{o}C, crystalline peaks of β-TCP appear and the peak intensities increase with calcination temperature. The appearance of β-TCP is owed to the dehydration reaction of hydroxyapatite. Two hydroxyl group forms one water and one oxygen vacancy at high temperature (>700 ^{o}C).

The weight percentage variation with temperature in Figure 2-3 also illustrate the same effect. The water in the samples exist in two forms, adsorbed water and lattice water. For hydroxyapatite powder, there is an outer layer of physically adsorbed water. The adsorbed water will be reversibly removed between 20 – 200 ^{o}C. Lattice water exists in the cracks, pores or connections of two single crystals of hydroxyapatite powder, and lattice water will be removed at approximately 400 ^{o}C. Both adsorbed water and lattice water account for the 2.13% weight loss. When the temperature exceeds 700 ^{o}C, hydroxyapatite will dehydrate to β-TCP, which accounts for the second weight loss in Figure 2-3.

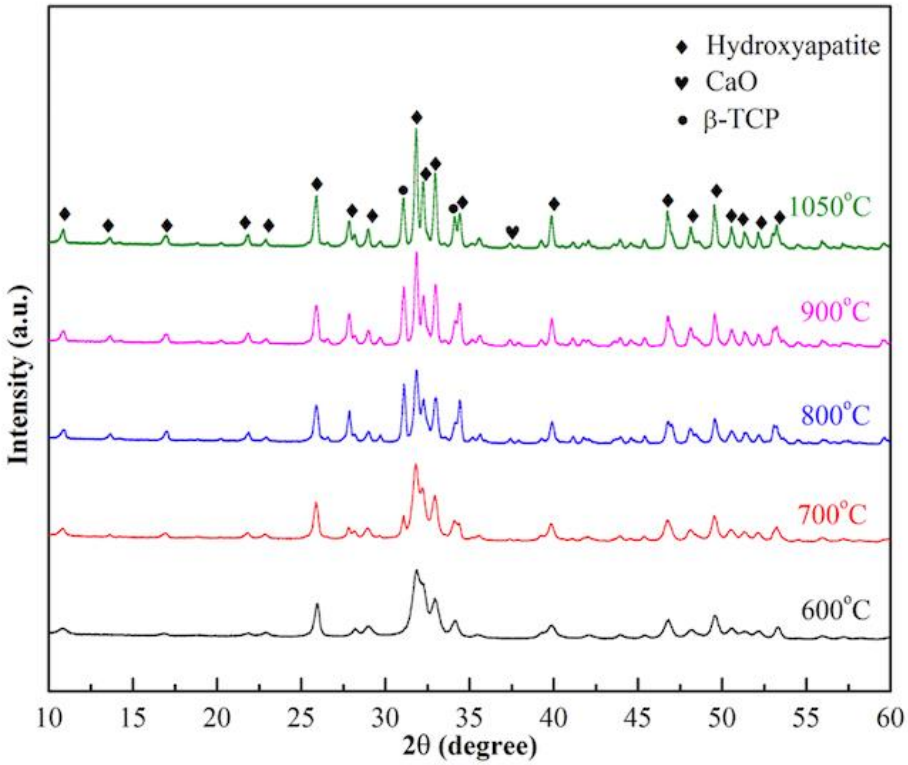

Figure 2-2. XRD patterns of hydroxyapatite calcined at 600 °C, 700 °C, 800 °C, 900 °C and 1050 °C.

These results are consistent with other works about the stability of hydroxyapatite.[66]

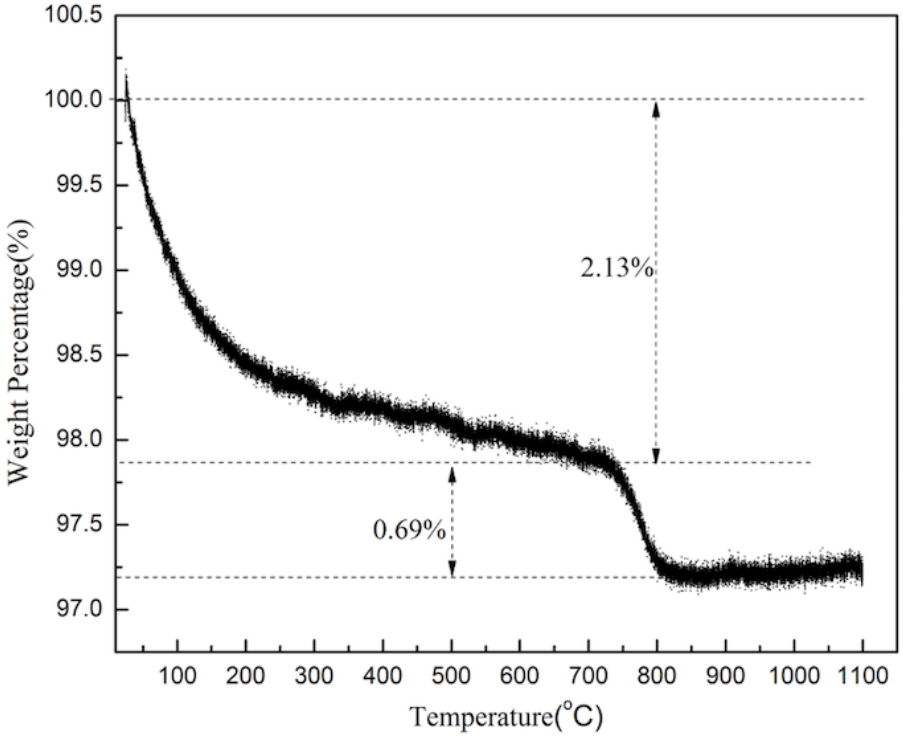

Figure 2-3. TGA of hydroxyapatite (600 ºC) without airflow.

2.2.5 Conclusions

Hydroxyapatite was successfully synthesized by chemical precipitation method. The thermal stability of HAP was investigated through X-ray diffraction and thermogravimetric analyzer. When the calcination temperature is higher than 700 ºC, hydroxyapatite will dehydrate to β-TCP, which was confirmed by XRD and TGA. However, most of the materials is still hydroxyapatite and impurities only account for a small percentage.

2.3 Solid State method

2.3.1 Materials

Calcium Nitrate Tetrahydrate (ACS, 99.0-103.0%) and Ammonium hydrogen phosphate (ACS, 98.0% min) were purchased from Alfa Aesar through VWR. Sodium bicarbonate (ACS 99.7%) was bought from BDH; Ethanol (absolute, anhydrous, ACS/USP grade) was purchased from PHARMCO-AAPER. All chemicals were used as received without any treatment. Deionized (DI) water was used for all purposes.

2.3.2 Experimental procedure

3.9632g $(NH_4)_2HPO_4$ and 3.3642g $NaHCO_3$ was mixed and ground by a small pestle and mortar for 30mins. Then 11.8092 g Ca(No3)2•4H2O was added and the mixture was ground for 1hrs. During this process, the solid mixture turned into paste and some bubbles emerged from the paste. After grinding, the sample was aged for 24 hours and then washed by ethanol and DI water separately. The samples were dried at 80 ^oC for 6 hours and then calcined at 550^oC, 650^oC, 750 ^oC, 850 ^oC and 950^oC for 3hours by a 1^oC/min heating rate. These samples are referred as ssHAP-550, ssHAP-650, ssHAP-750, ssHAP-850 and ssHAP-900 respectively. The sample that were not calcined was termed as ssHAP-25. The characterization methods were the same as 2.2.3.

2.3.3 Results and Discussion

The morphologies of hydroxyapatite samples are shown in Figure 2-4. Without calcination (Figure 2-4 A-ssHAP-25), most of the particles aggregated. The agglomeration is attributable to the incomplete removal of water inside the particle in the calcination process or the growth of small particles on clusters during the mixing of reactants. After calcination at 550 and 600 ^oC, some particle clusters existed, but much

less than ssHAP-25. Particle shapes were not uniform. The sizes of ssHAP-550 were ~100nm and ssHAP-650 ~200nm. Compared with ssHAP-650, the particle size of ssHAP-750 and ssHAP-850 did not change recognizably. Morphologies of particles varied, but several platelet particles appear, which are the main shapes as in Xiaojun Guo's work[40]. The SEM image of ssHAP-900 exhibited uniform, rod-like structure and the particle size is roughly 500 nm. The SEM images of different calcination temperature indicate that increasing the calcination temperature increase the particle's size, and the particle shape changed.

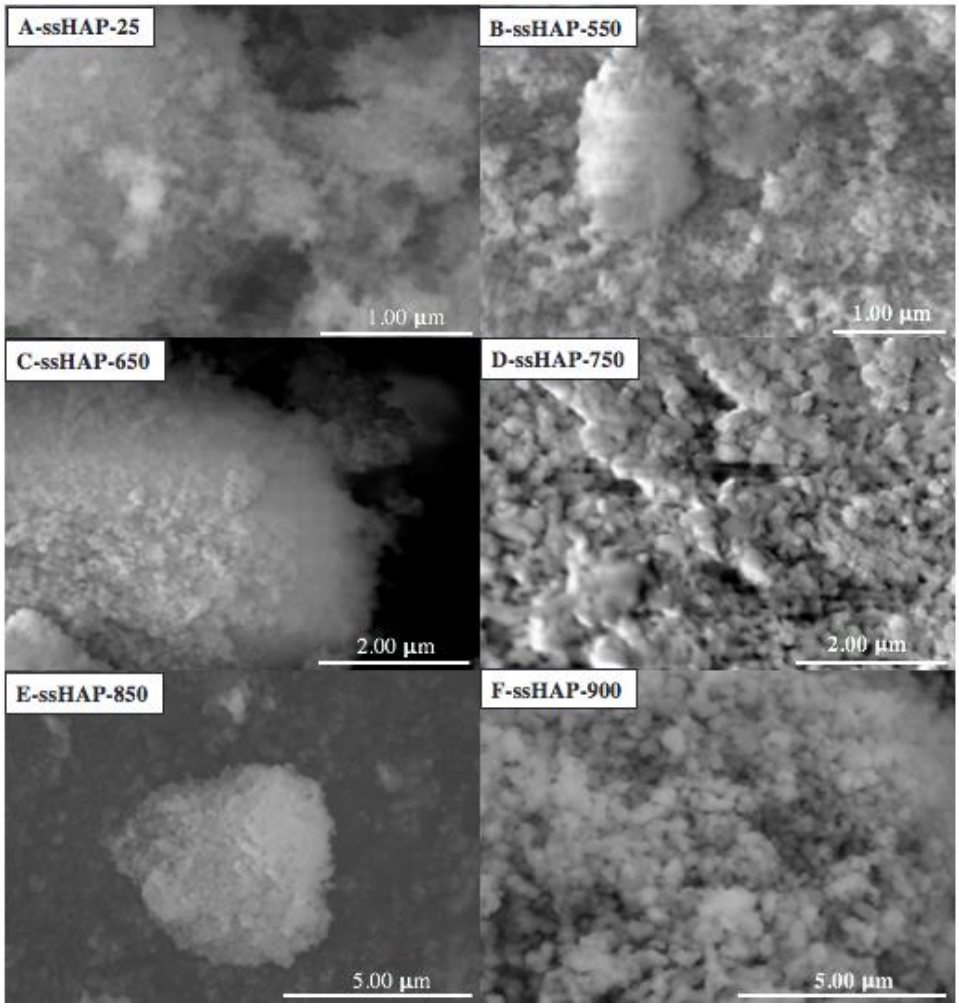

Figure 2-4. SEM images of ssHAP-25(A), ssHAP-550(B), ssHAP-650(C), ssHAP-750(D), ssHAP-850(E), and ssHAP-900(F).

Table 2-2 exhibits the surface area and particle size of hydroxyapatite calcined between 25 and 900 ^{o}C. The Change of calcination temperature modified the surface area from 66. 971 m^2/g to 6.039 m^2/g and particle size from 146.17 nm to 253.55 nm. These particle sizes differed from the sizes determined by SEM images in Figure 2-2, although both reveals that particle enlarge. The aggregation of particles could explain the difference. The particle size measured by Light Scattering is the size of a cluster of particles suspended in solution. When clusters dissociate, and single crystals exist, the sizes measured by DLS and SEM will be the same. The increase of surface area is consistent with the decrease of particle size.

Table 2-2. Surface area and particle size of solid state reaction hydroxyapatite calcined at different temperatures.

Calcination Temperature(^{o}C)	Surface area (m^2/g)	Particle size/radius(nm)
25	66.971	385.34
550	28.421	146.17
650	17.274	147.25
750	9.535	185.90
850	8.560	211.05
900	6.039	253.55

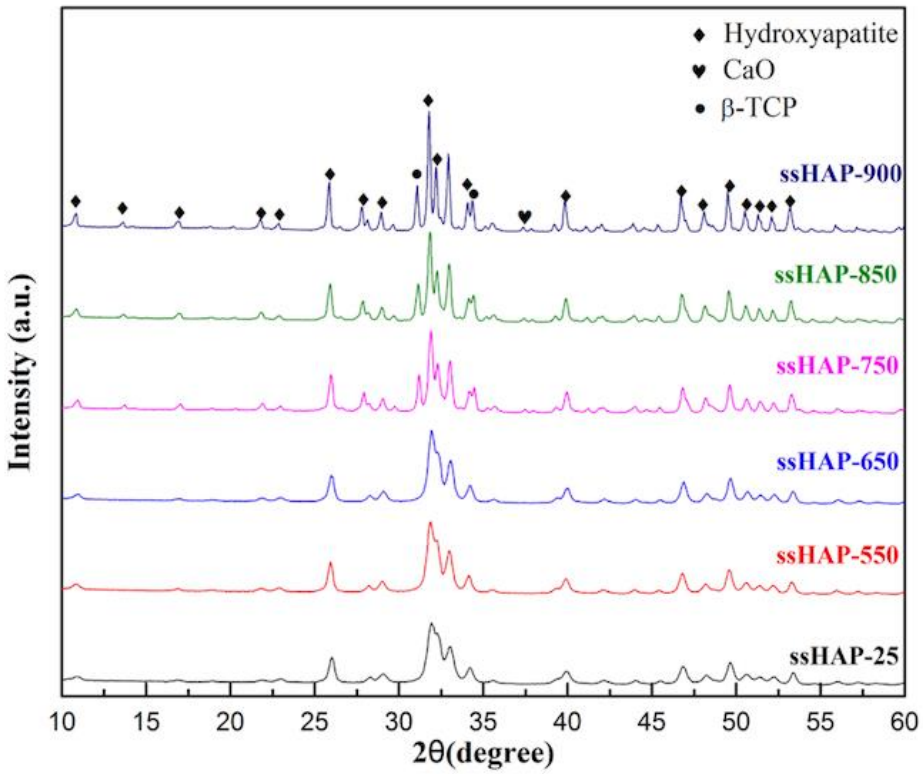

Figure 2-5. XRD patterns of hydroxyapatite calcined at 25 ºC (ssHAP-25), 550 ºC (ssHAP-550), 650 ºC (ssHAP-650), 750 ºC (ssHAP-750), 850 ºC (ssHAP-850), 900 ºC (ssHAP-900).

The X-ray diffraction patterns of solid state synthesized hydroxyapatite calcined at different temperatures are shown in Figure 2-5. All of the samples display the typical peaks of hydroxyapatite[57]. The characteristic peaks of hydroxyapatite, including peaks at 26º (002) and 30-34º (211, 112, 300), are observed. When the calcination temperature is low (550 and 650 ºC), the peaks are broad, which indicates crystallinity is low. The low crystallinity is due to the incomplete reaction between reaction precursors. No other peaks corresponding to other calcium phosphate apatites were detected. The absence of additional peaks reveals that those samples comprise pure hydroxyapatite. With the increasing calcination temperature, peaks became sharp and peak intensities increased, which represents the growing crystallinity of the materials. Except for the peaks of hydroxyapatite, some other peaks appear. The peak at 31.8º corresponds to β-TCP and

the peak at 35° corresponds to CaO[40]. The appearance of these peaks is due to the dehydration of hydroxyapatite at high temperature. Therefore, higher calcination temperature (>650 °C) will lead to the dehydration of hydroxyapatite and adds impurities to the samples. Higher calcination temperature broadens the hydroxyapatite peaks, increases the crystallinity and leads to impurities. The intensity and sharpness of hydroxyapatite peaks also reveal the increase of particle size based on the Scherrer equation[67]. The broader the peaks, the smaller the particle size. This phenomenon also agrees with the size variations with the calcination temperature indicated by XRD and particle size measurement.

2.3.5 Conclusions

HAP materials were successfully synthesized by the room temperature solid state method. Calcination determines the properties of hydroxyapatite. Calcination increases the crystallinity and particle size, but also leads to impurities when the temperature is higher than 650 °C. Although the solid-state method produces hydroxyapatite with different particle sizes and shapes, this method was not applied in the future work due to the time-consuming preparation procedure and low productivity.

Chapter 3: Hydroxyapatite membrane synthesis

3.1 Introduction

Ceramic membrane could be manufactured into disk, monolithic multi-channel, tubular (dead end or not) or hollow fiber configurations. Disk membranes are generally used in the lab since they could be easily prepared by conventional pressing method and characterization of disk membranes is also simpler compared with other shapes. Multiple tube membranes could be assembled into a module and then applied in both research laboratory and industry. Both disk and tubular configurations have a small surface area to volume ratio, which indicates the separation area per unite membrane volume. To increase the surface are to volume ratio, hollow fiber and monolithic multi-channel structures are designed. The surface area to volume ratio of the former one could be up to 3000 m^2/m^3 and the latter one could be up to 800 m^2/m^3 [17]. For the multi-channel monolithic form, the bulk is a porous support to provide mechanical robustness and separation layer is fabricated on the inner channel. Therefore, the feed will flow through the inner channel and the permeate will flow through the inner separation layer then the porous bulk to the surface of the membrane. Hollow fiber membranes have the highest surface area to volume ratio and then the highest packing density. These four ceramic membranes could all be dense or porous and that depends on the materials and preparation methods. In our work, hydroxyapatite membranes were fabricated into disk by conventional pressing, tubes by tape casting methods and hollow fibers by phase inversion method through both single orifice and coaxial office spinneret. Each of them are discussed in details below.

3.2 Hydroxyapatite flat membrane

Power pressing is the first method that people make ceramic tiles and other high density products. There are two types of powder pressing method, axial pressing and isostatic pressing. Axial pressing could be further divided into dry and wet pressing. For dry pressing, only powder is used. Solvent especially water is added in the wet pressing. For axial pressing, the applied pressure on the powder comes from one direction. Isostatic pressing supplies multiple directions forces on the powder to achieve higher uniformity of compression and shape. Typically, for powder processing, powder or power mixture with additives are poured into a metal modulus and then punched at certain temperature and pressure (Figure 2-1[18]). After that, the pellet is sintered to finalize the membrane. Due to its simplicity and low cost, powder pressing is widely used in the lab for simple geometrical shapes. In this work, hydroxyapatite pellet was also fabricated through dry powder pressing method.

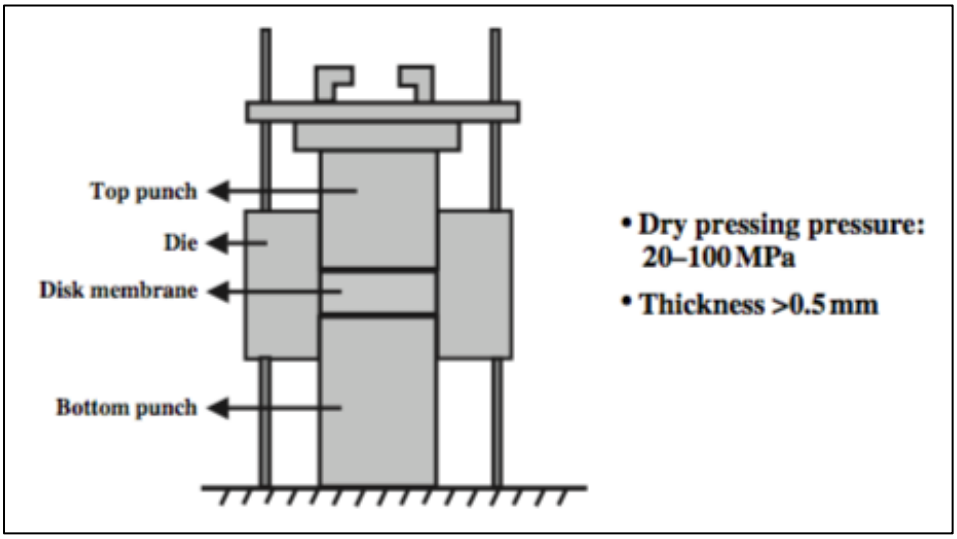

Figure 3-1. Powder pressing.

3.2.1 Materials and experiment procedure

Hydroxyapatite powder was synthesized by chemical precipitation method as mentioned in chapter 2. After calcined at 600 ^{o}C for 6 hours with airflow, the powder was ground below 80 mesh. 1.4 g powder was pressed into pellet by *CARVER HYDRAULIC UNIT* (model #3912) for 3mins by 3000 psi. The pellet was sintered at 1250 ^{o}C for 4 hours for solidification.

The morphologies of the membrane were recorded by scanning electron microscopy (SEM) on a Hitachi SU-70 electron microscope.

3.2.2 Results and Discussions

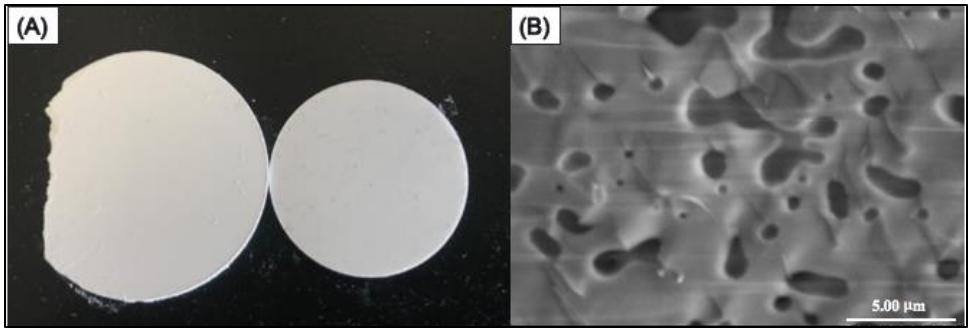

Figure 3-2. Images of Hydroxyapatite pellet. (A) pictures of pellet. Left: before calcination; Right: after calcination; (B) SEM image.

Hydroxyapatite pellets was prepared by dry pressing method and pellet picture and SEM image is shown in Figure 3-2. The green body was a pellet with 2mm depth and 2.86 cm diameter (the missing part is due to fragility). After sintering at 1250 ^{o}C, the diameter changed into 2.29cm and the shrinkage is 19.93%, which is a result of sintering effect. Pellet surface was smooth and no crack was observed. Scanning electron microscope image (Figure 3-2 (B)) shows that the surface is not flat and some pinhole exists. The pinhole may arise from the heterogeneity of hydroxyapatite particles or dehydration of water of hydroxyapatite to TCP at high temperature. The pinhole existence could not determine whether the pellet is porous. Hydroxyapatite pellet has

already been explored broadly in the research about the stability and sintering properties of hydroxyapatite. Our research will focus on other shape hydroxyapatite membranes.

3.3 Hydroxyapatite tubular membrane by tape casting method

Tape casting is a common method to prepare flat sheet ceramic membrane. As shown in the schematic of tape casting (Figure 3-3), ceramic slurry in the container is casted on the moving tape by a doctor blade, followed by a solvent evaporation process in a drying chamber to form green tape. Green tape could be used as a single layer or patterned, stacked and laminated to form three dimensional structures[68]. In our work, the green tape was rolled into a tube with a stainless-steel tube. Like other membrane preparation methods, sintering is the last step of tape casting to form porous or dense ceramic membrane. Thickness of the membrane ranges from 1μm to 3000 μm by adjusting the distance of doctor blade and moving tape[69]. Properties of tape casting membrane are determined by ceramic slurry (like contents of each components, viscosity) and machine condition (reservoir depth, speed of carrier, doctor blade height. etc.). These factors influence the final properties of flat sheet by changing the rheological behavior of the moving ceramic slurry[70]. For example, carrier speed has a significant influence on the tape thickness and high speed will result in thin slip tape.

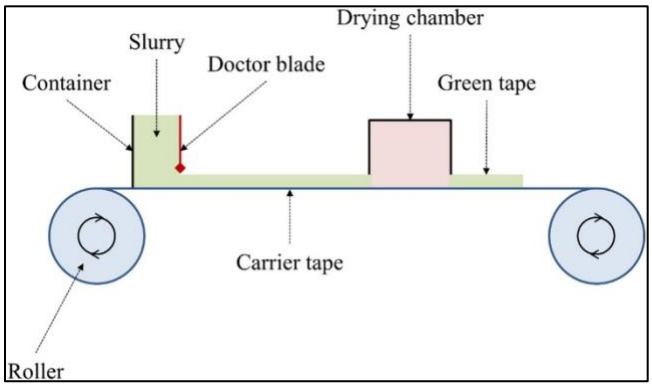

Figure 3-3. Schematic of tape casting.[71]

The first step of the tape casting is preparing ceramic slurry. Typically, a ceramic slurry contains ceramic powder, solvent, binder, dispersant and plasticizers or sintering agents. Solvent disperses particles and dissolve additives to form the slurry. After tape casting, solvent evaporation forms the green body. Solvent could be water and organic solvents like ethanol and toluene. Grain clusters formed during the mixing process, which are results of original grain cluster or grain agglomeration. The clusters produce uniformity of the suspension and cracks in the final membranes. Dispersant increases the electrostatic repulsion in the slurry by coating dispersant molecule on the ceramic particles. Common dispersants comprise soda ash, sodium silicates, olyacrylates, polyehtyleneimines, menhaden fish oil, phosphate ester[72, 73]. Solvent evaporation might change the plasticity or shapes of membrane. Binders and plasticizers are used to keep the morphologies of green body before drying and prevent cracking at sintering. Binder could wet the surface of grains by physically adsorption or chemical adsorption through organic functional groups on the particles. An ideal binder should lubricate the slurry, strength the green body, be inexpensive and non-toxic and totally decompose at 300-500 ^{o}C without no ashes[74]. Lots of polymers could act as binders, such as polyvinyl butyral (PVB), poly (butyl methacrylate) (PBMA) and poly (propylene carbonate) in organic

solvent slurry and starch and polyvinyl alcohol (PVA) in aqueous suspension. By infiltrating into the long chain of binders, plasticizers could improve flexibility of binders in the slurry, enhance the elasticity of green body and preclude the cracking in the sintering. Conventional plasticizers include ethylene glycols, glycerol, polyethylene glycols and Benzyl Butyl Phthalate[75, 76]. Other additives like pore former, lubricants and antifoam agents are added sometimes but not very common[12].

3.3.1 Materials

Menhaden fish oil, Polyvinyl butyral and Benzyl Butyl Phthalate as tape casting specialists were all bought from Tape Casting Warehouse, Inc. Ethanol (absolute, anhydrous, ACS/USP grade) was purchased from PHARMCO-AAPER. 80 mesh-hydroxyapatite powder (calcination at 900 ^{o}C for 4 hours) was prepared by chemical precipitation method. All chemicals were used as received without any treatment and Deionized (DI) water was used in all purpose.

The morphologies of the membrane were recorded by scanning electron microscopy (SEM) on a Hitachi SU-70 electron microscope.

3.3.2 Experimental procedure

The hydroxyapatite slurry for the tape casting process were prepared by mixing 40 g hydroxyapatite powder and 2 g Menhaden fish oil (dispersant) in ethanol and the mixture was ball milled for 24 hours. 6.5 g Polyvinyl Butyral (binder) and 4 g Benzyl Butyl Phthalate (plasticizer) were added into the mixture and then ball milled for 48 hours. The slurry was used for tape casting. The ceramic tape was dried for around 2 hours. The membrane could be rolled into tube structure through a stainless-steel rod.

The tube or flat membrane was sintered at 800 °C, 900 °C and 1250 °C for 4 hours to form high-strength membrane or tube.

3.3.3 Results and Discussions

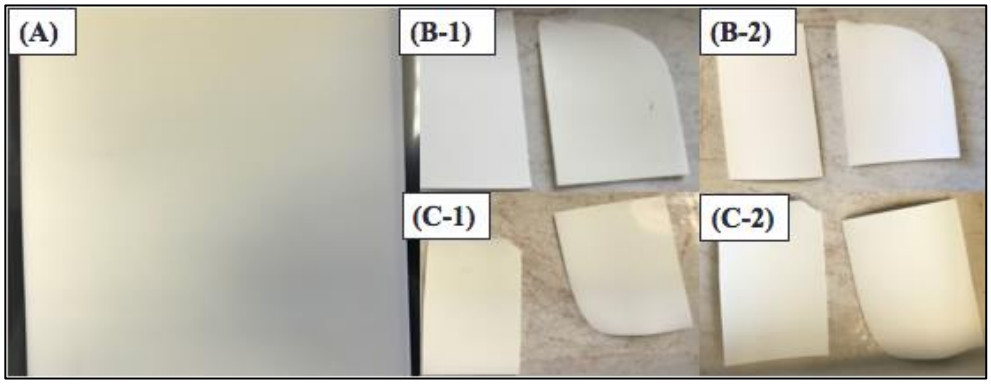

Figure 3-4. Pictures of Hydroxyapatite tape membrane before and after calcination. (A) Dry membrane; (B-1) before calcination at 800 °C; (B-2) after calcination at 800 °C; (C-1) before calcination at 900 °C; (C-2) after calcination at 900 °C.

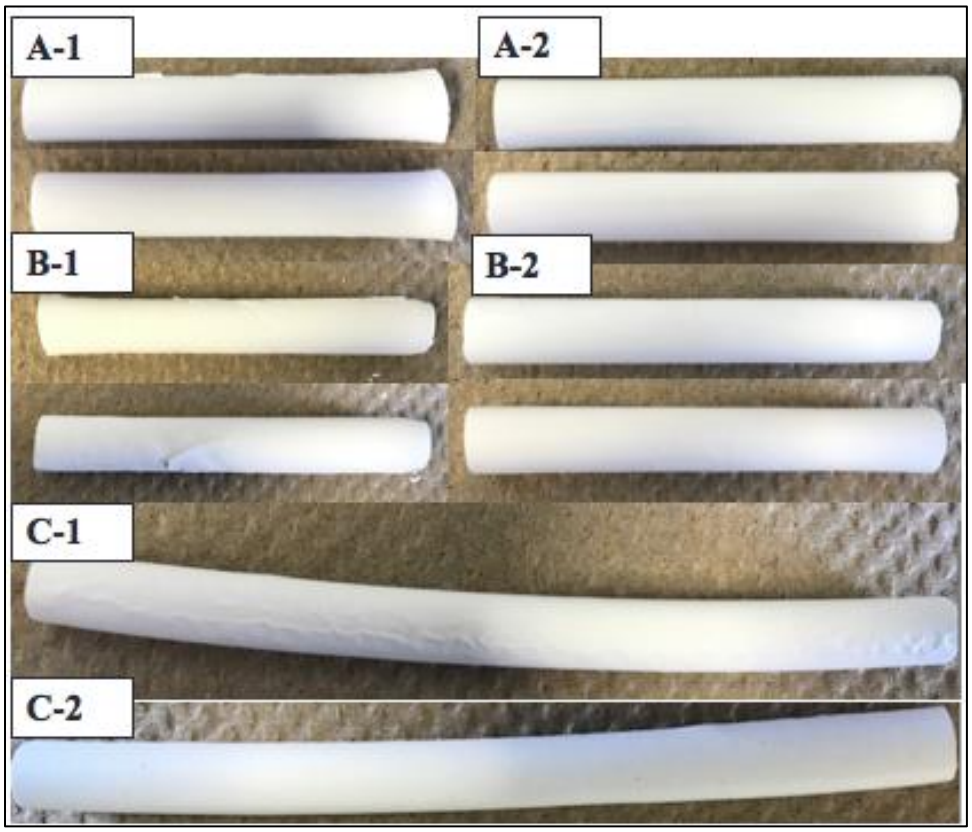

Figure 3-5. Pictures of Hydroxyapatite tube membrane. (A-1) before calcination at 800 °C; (A-2) after calcination at 800 °C; (B-1) before calcination at 900 °C; (B-2) after calcination at 900 °C; (C-1) before calcination at 1250 °C; (C-2) after calcination at 1250 °C.

Morphologies of green body and flat membranes sintered at 800, 900 and 1250 ^{o}C are shown in Figure 3-4. The green body of flat membrane was smooth (A in Figure 3-4). The surface of sintered membranes was smother than before sintering and the sheet membrane hardened. Sintering does not lead to any cracks on the surface of the membrane (B and C in Figure 3-4).

Flat sheet was laminated into the tubular shape to prove the flexibility of the green membrane. As shown in Figure 3-5, uniform and symmetric tubular structures were formed. Outside layer were smooth and no cracks formed in the rolling process, except for some folding at the edge of original sheet, which was due to the inappropriate rolling and the thin layer at the edge of the rolling membrane. The sintering process solidified the tube without any cracks (A-2, B-2 and C-2 in Figure 3-5). The shrinkage ratio increase with higher sintering temperature. Axial length decrease by 20.64 % when the membrane was fired at 1250 ^{o}C, which is larger than the shrinkage ratio of 19.89 % and 16.73% at 800 ^{o}C and 900 ^{o}C respectively (the difference is due to measurement error). These results confirm the flexibility of green body membrane of hydroxyapatite and the success of the tape casting process to form hydroxyapatite flat sheet.

SEM images of the surfaces of the membrane sheet sintered at 800 ^{o}C and 900 ^{o}C and tube membrane sintered at 1250 ^{o}C are shown in Figure 3-6. When the membranes were calcined at lower temperatures (800 and 900 ^{o}C), the membrane had a crack- free and porous surface with vague grain boundaries (A and B in Figure 3-6). No particle coalescence or grain growth could be observed. The sintering effect is low due to the low temperature. The sintering effect turned strong at a higher temperature (1250 ^{o}C). There are clear grain boundaries and the grain size grew to approximately 1- 3μm, which is

larger than the grain size in the lower temperature and the particle sizes in the slurry. The surface of the membrane is not flat and some pinholes exist, but the membrane is still dense, based on the dense sintering SEM image in Figure 3-6 C-2.

Water permeation test further proved that the membrane was dense. The experiment setup is shown in Figure 3-7. By using a similar setup in the literature[77], a one side dead end tube membrane was immersed in water, and the other side was connected to vacuum pump. The vacuum is 0.33 bar and permeated water will be collected in permeate collector as shown in Figure 3-7.

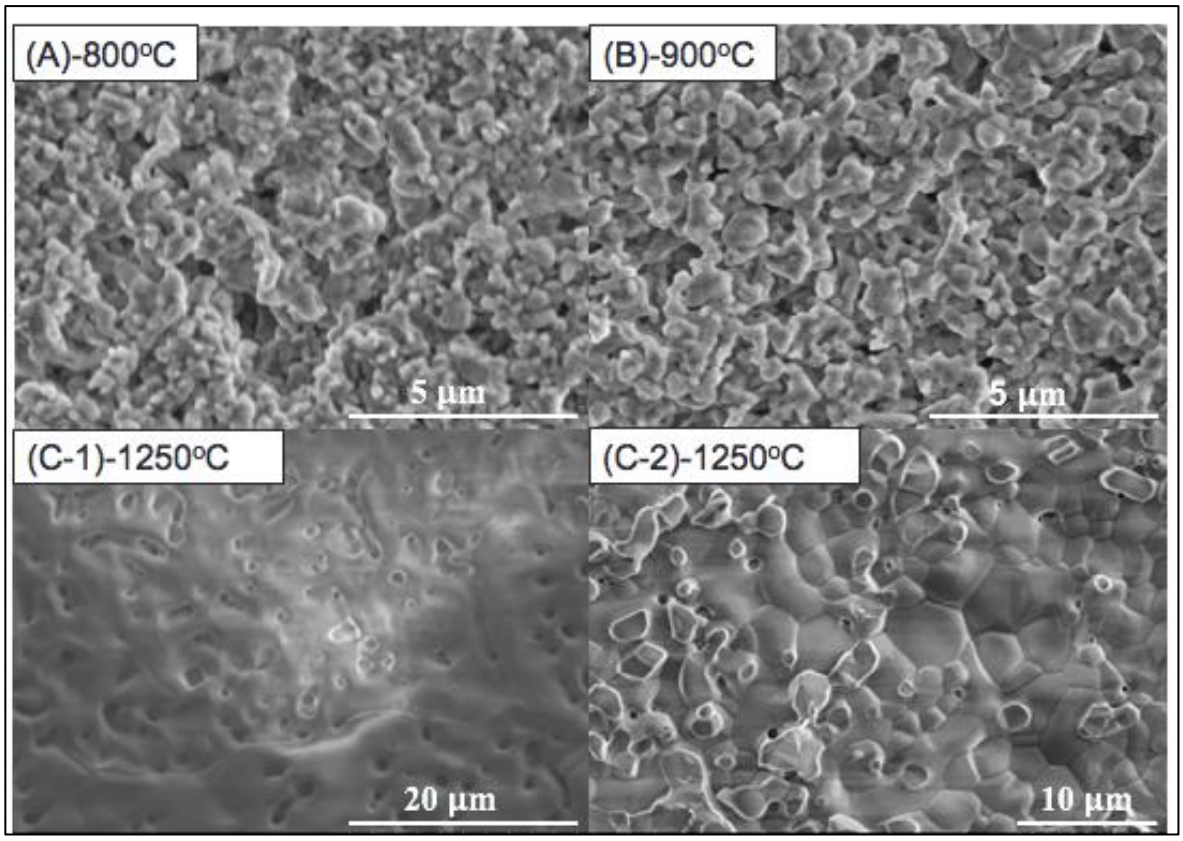

Figure 3-6. SEM image of sintered hydroxyapatite tube membrane. (A-800°C) outer surface after calcination at 800 °C; (B-900°C) outer surface after calcination at 900 °C; (C-1-1250°C) outer surface after sintering at 1250 °C; (C-1-1250°C) inner surface after sintering at 1250 °C.

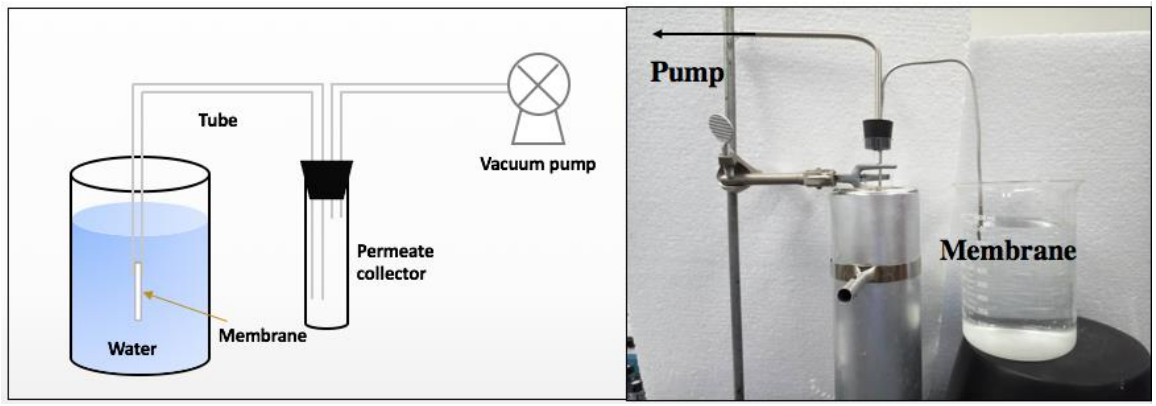

Figure 3-7. Membrane water filtration setup.

The results are presented in Table 3-1. A dense commercial Al_2O_3 was utilized as a control. Comparing the collected water at the same time (~3hr 20min) with the control membrane, hydroxyapatite tube prepared by tape casting method had little water detected and the fluxes for both membranes approximated zero. The water collected possibly came from residual water in the stainless-steel tube or permeate collectors. This result further proved that the membrane is dense or at least non-permeable for water.

Table 3-1. Permeation results of prepared HAP (sintered at1250 ^oC) and commercial ¼ inch dense Al_2O_3 tube.

Sample	△m/g	Duration time	Flux J/(g/(m^2*min)
HAP tube	0.11	3hr 20 mins	~0
Al_2O_3 tube	0.07	3hr 18 mins	~0

3.3.4 Conclusions

A dense hydroxyapatite tube membrane was successfully synthesized by tape casting method. No cracks formed on the green membrane and membranes sintered at 800, 900 and 1250 ^oC. SEM images showed clear grain boundaries caused by sintering and revealed the surface were dense. A water permeation setup was built to further

demonstrate that the membrane is dense by comparing the permeated water over a long time with commercial a Al_2O_3 tube.

3.4 Hydroxyapatite hollow fiber membrane by phase inversion through single orifice

3.4.1 Introduction

In membrane separation process, an important factor for the separation membrane is the surface to volume ratio, since that ratio determine separation area per unit volume and influence the packing of membranes. The surface to volume ratio of hollow fiber membrane could reach 3000 m^2/m^3[318], which is the highest ratio compared with other configurations membranes. Hollow fiber membrane is one kind of tubular membranes with small outer and inner diameters. In general, the internal diameter ranges between 40~300 μm and wall thickness between 10~100 μm[78]. Hollow fiber membrane is generally prepared by combination of spinning method and phase inversion. The first step for this method is the ceramic slurry preparation. Ceramic slurry containing ceramic powder, solvent and polymer additives is homogenized, then extruded into non-solvent through a concentric orifice spinneret with bore liquid forced flow through the inner lumen of the hollow fiber. During the extrusion process, phase inversion occurs and solidifies the slurry to form green hollow fiber membrane. Phase inversion and spinning determine the morphologies and properties of hollow fiber membranes and spinning affects the properties through its influence on phase inversion process. Therefore, phase inversion process is the key factor that controls the hollow fiber membrane properties.

Table 3-2. Comparison of different structure membranes[79].

	Hollow fibre	Plate-and-frame	Tubular
Cost/area	Low	High	Low
Membrane replacement cost	Moderate	Low	Moderate/low
Flux(l/(m^2*h))	Good	Low	Low
Packing density(m^2/m^3)	Excellent	Good/fair	Good
Hold-up volume	Low	Medium	Medium
Cleaning in place	Good	Fair/poor	Fair/poor

Phase inversion is a "demixing" process whereby polymer or ceramic slurry is transformed from a solution state to a solid state. Phase inversion could be initiated by a range of different factors, such as thermal variation, evaporation and addition of a non-solvent[80]. Addition of a non-solvent or immersion precipitation is most widely used to activate the phase inversion. With addition of non-solvent, the thermodynamically stable binary system between solvent and polymer or ceramic slurry is disturbed. The new ternary system is not stable and the appearance of demixing solidifies the polymer or ceramic slurry to form a green membrane. If the demixing occurs instantaneously after addition of non-solvent, the green membrane with a relatively porous top layer will form. In contrary, if the demixing is delayed after mixture of solvent and non-solvent, the top layer will be comparatively dense. Exchange between solvent and non-solvent leads to the formation of polymer rich phase and polymer lean phase. Polymer rich phase forms membrane matrix and polymer lean phase becomes membrane void[81].

Phase inversion by immersion precipitation uses a coaxial spinneret with bore liquid flow inside to form hollow structure. Bore liquid supports to shape the inside channel of the hollow fiber and affects the inner wall structure. Diameter of hollow fibers

is limited by the size of the coaxial spinneret, which could not be very small considering manufacture difficulty and price of two coaxial tubes. However, the smaller the diameter of hollow fiber, the larger the surface to volume ratio and separation efficiency. Therefore, how to reduce the size of hollow fiber attracts considerable interest. One feasible method is to use a single orifice spinneret. The key of synthesizing hollow fibers through single orifice spinneret lies in the formation of the hollow structures. A novel method was proposed to utilize oil as inner channel former assistance to construct the hollow structure[82]. As shown in Figure 3-8, the oil added in the ceramic slurry diffuses into the center of green membrane during the phase inversion process due to its immiscibility with water and followed oil removal forms the hollow structure. This method was used in our work to synthesize hydroxyapatite hollow fiber through a single orifice spinneret and dodecane was used as oil for the formation of hollow structures.

3.4.2 Materials

Hydroxyapatite powder (80 mesh) prepared by chemical precipitation method; Polysulfone (PS, pellets, M_w ~ 35,000 by LS) and Dodecane (anhydrous, 99+%) was purchased from *SIGMA-ALDRICH*. 1-Methyl-2-Pyrrolidinone (NMP, SEMI Grade) was purchased from BDH. Polyvinylpyrrolidone (K 30 MW. av. 40000) was purchased from TCI. Ethanol (absolute, anhydrous, ACS/USP grade) was purchased from PHARMCO-AAPER. All chemicals were used as received without any treatment and Deionized (DI) water was used in all purpose.

3.4.3 Experimental procedure

Hollow fiber was prepared by phase inversion method through the single orifice. 1.5g Polysulfone was mixed with 8.5g NMP and then stirred for 2 hours at 60 ^{o}C. 1.0g

dodecane was added and continuously stirred for another 2 hours. 5 g hydroxyapatite powder was slowly added to the mixture and then stirred for 48 hours. The suspension was degassed for 30 mins and then extruded into hollow fiber by equipment setup shown in Figure 3-8[82]. The ceramic polymer mixture solution was pumped into water vertically by 2.4 ml/min through 22G (ID: ~0.41mm) and 16G needle(ID:1.19mm). The fresh hollow fiber was immersed in water overnight to form steady structure and then kept in ethanol (~50 ^{o}C) for 2hrs to remove the dodecane. After drying at 80 ^{o}C for 6 hours, the hollow fiber was sintered at a Sentro Tech High Temperature Furnace with the following program: heated up to 600 ^{o}C by 2 ^{o}C/min for 4 hours and then to 1250 ^{o}C by 2 ^{o}C/min for another 4 hours, finally cooled down to RT by 5 ^{o}C/min. The sintered hydroxyapatite hollow fiber was used for characterization.

The morphologies of the membrane were recorded by scanning electron microscopy (SEM) on a Hitachi SU-70 electron microscope.

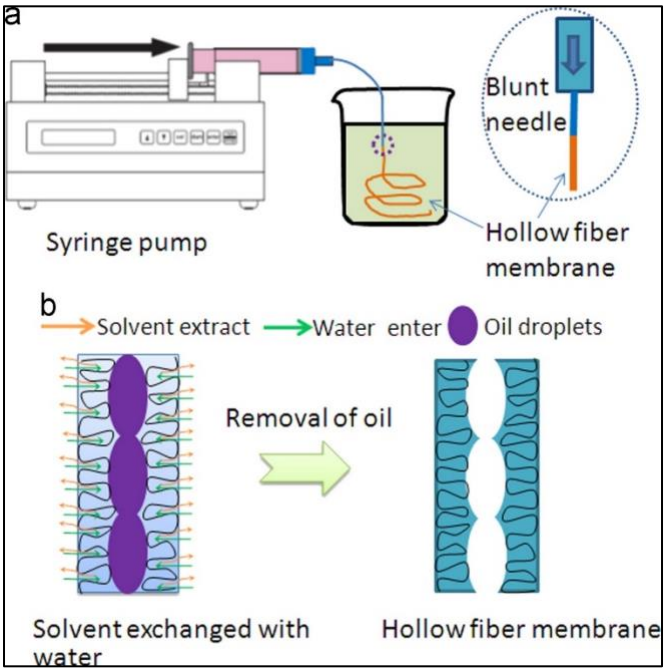

Figure 3-8[82]. Schematic diagrams of (a) phase inversion spinning of ultrafine hollow fiber membranes through a single syringe tip, and (b) the formation of hollow fiber membranes via phase separation process.

3.4.4 Results and Discussions

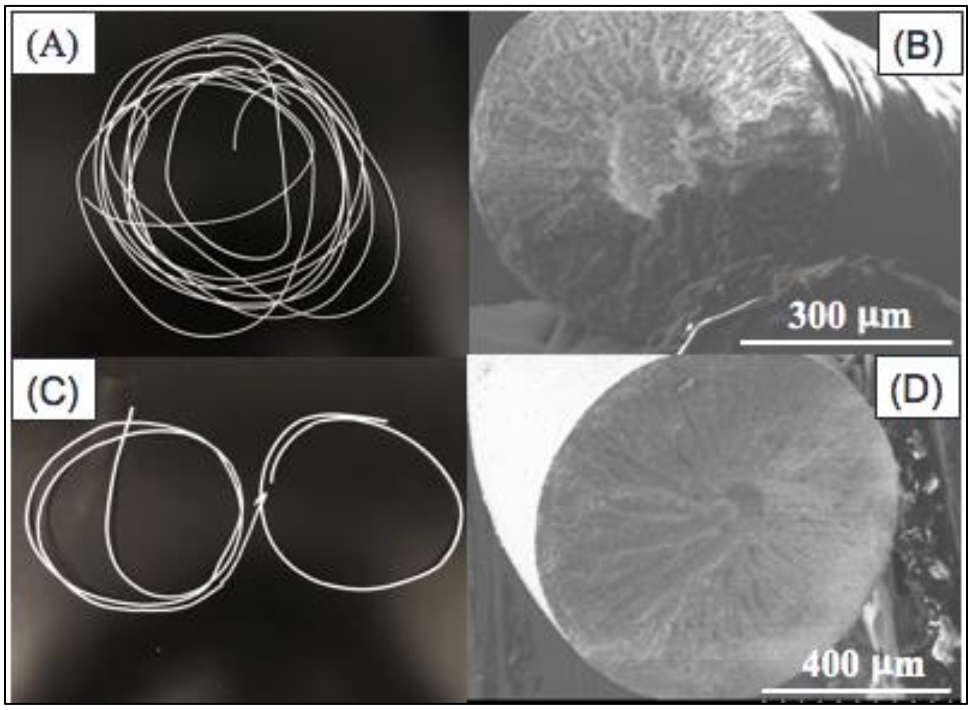

Figure 3-9. Pictures and SEM images of 16G and 22G hydroxyapatite hollow fiber. (A) 22G hollow fiber picture; (B) SEM image of 22G hollow fiber; (C) 16G hollow fiber picture; (D) SEM image of 16G hollow fiber.

The morphologies of the hydroxyapatite hollow fiber are shown in Figure 3-9 and Figure 3-10. A and C in Figure 3-9 are the digital photos of hydroxyapatite hollow fiber through 22G and 16G needle respectively. Long uniform membranes with smooth outer surface were formed. SEM images of the cross section of the membrane in Figure 3-9 C and D exhibits the channel formed by oil droplet. Small oil droplet in the ceramic slurry agglomerate and diffuse to the center of the tube due to the solvent exchange of NMP and water. After the immersion of green tubes in the ethanol, oil was dissolved in ethanol and a droplet hollow structure formed. Compared with hollow fibers extruded through coaxial orifice spinneret, long extended finger like macrovoids also formed when only one orifice spinneret was used. Solvent and non-solvent exchange leads to the ceramics rich phase

and ceramics lean phase. The ceramics lean phase became the microvoid structure during dry and sintering process.

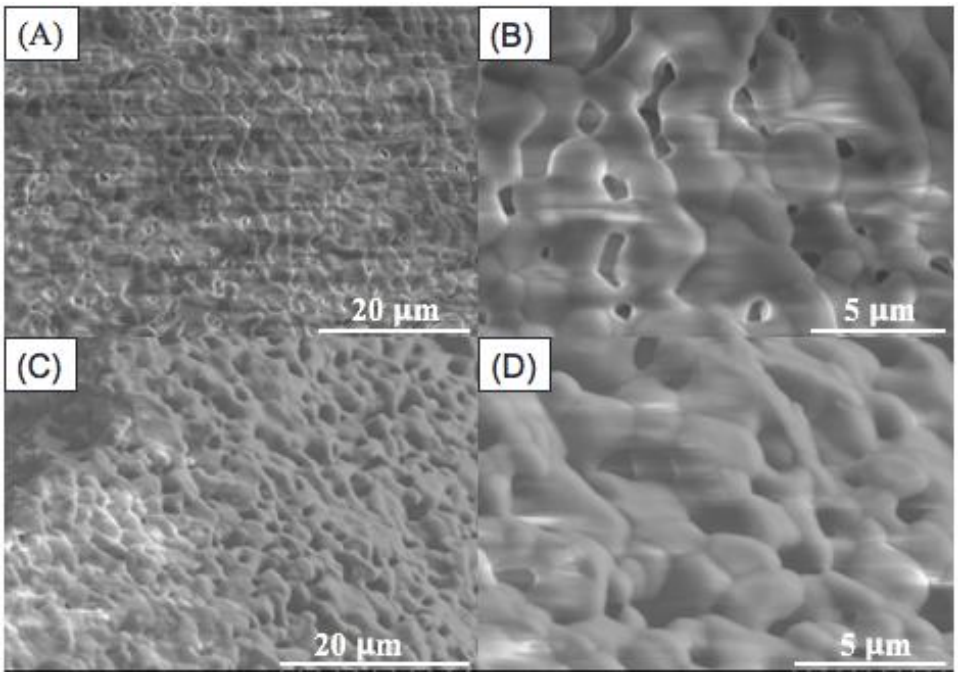

Figure 3-10. SEM images of outer surface of 22G and 16G hydroxyapatite hollow fiber. (A) and (B): 22G; (C) and (D): 16G.

Figure 3-10 shows the surface structure of 22G and 16G hollow fiber membrane. Both membranes have a porous thin top layer, which was formed during the instantaneous liquid-liquid demixing in the phase inversion process. In the polymer membrane formation by phase inversion method, two types of liquid-liquid demixing exist during the phase inversion process, instantaneous liquid-liquid demixing and delayed onset of liquid-liquid demixing[80]. For the instantaneous liquid-liquid demixing, membrane forms in the time order of one second or less. The top layer is very thin and the sublayer is full of macroviods. For the delayed liquid-liquid demixing, the precipitation time is in the order of seconds to minutes and the top layer will be dense and thick[83]. Even though ceramic slurry is different from the polymer mixture, ceramic

particles coated with polymer addictive are similar to polymer. Therefore, the top thin porous layer could be explained by the instantaneous liquid-liquid demixing process.

3.4.4 Conclusions

Hydroxyapatite hollow fiber membrane was synthesized by phase inversion method through a single orifice. Dodecane added into the ceramic slurry diffused into the center of the membrane due to the water and NMP exchange. A droplet channel formed during the phase inversion process. Only SEM images could not prove the inner channel is through. More experiments like XuM or permeation test is needed to further verify that hollow fiber is not blocked.

Chapter 4: Hydroxyapatite hollow fiber membrane

4.1 Introduction

As mentioned above in chapter 3.4, extrusion of the ceramic slurry through coaxial spinneret is more widely used than single orifice spinneret. The addition of bore liquid sustain the formation of hollow structure as a support and phase inversion between the solvent and bore liquid provides a method to modify the inner structure of the hollow fiber. Furthermore, compared with the single orifice method above, the coaxial spinneret method ensures the formation of the through hollow fiber without. The phase inversion method through a coaxial spinneret to synthesis hydroxyapatite hollow fiber was discussed in this Chapter.

The application of hydroxyapatite hollow fiber membrane in oil water separation was also presented in this chapter. As mentioned in chapter 1, for membrane separation in oily water separation, oil droplet size is an important factor that determines the requirements of the membrane. Several forms of oil and grease exist in the oily water, including free, disperse or emulsified oil. The criteria for classification is the droplet size. The droplet size of free oil is greater than 180 μm and dispersed oil ranges from 120 to 150 μm. The oil with droplet size smaller than 20 μm is classified as emulsion oil. Free and disperse oil droplet could be removed by conventional separation method or pretreatment method. Emulsion oil is hard to separate and membrane technology is required to separate oil from the water to reach discharge requirements. The oil water

sample used in this work is emulsion oil by mixing n-dodecane, sodium dodecyl sulfate and water, which was reported before[84].

In the membrane separation process for oily water, one of the major hindrances is fouling, which prevents the commercial application of membrane. During the continuous membrane operation, if the flux through the membrane is kept constant, the transmembrane pressure will increase and flux will decrease when the transmembrane pressure is uniform. The reason for this phenomenon is fouling. Fouling is the process that lead to the loss of performance of a membrane caused by the deposition of suspended or dissolved substances on its external surfaces, at its pore openings, or within its pores[85]. Fouling leads to severe effects on the membrane performance and then cleaning is needed. Membrane cleaning is defined as process to remove the substances that don not belong to the membrane itself. Cleaning include physical cleaning and chemical cleaning. Chemical additives help to cure the membrane fouling during the chemical cleaning, and the physical cleaning is done by flushing, mechanical scouring, electrical cleaning and relaxation. The fouling that could be cured by physical cleaning is reversible cleaning and that requires chemical cleaning is irreversible cleaning. Therefore, the whole membrane operation process should be normal operation-fouling-cleaning-integrity test. For ceramic membrane, a simple and high-efficient cleaning method is calcination to remove all organics deposited on the membrane due to the high stability of ceramics. In this work, the used hydroxyapatite hollow fiber membrane was regenerated by calcination and the oil removal efficiency of the new membrane were also discussed.

4.2 Experimental

4.2.1 Materials

Calcium Nitrate Tetrahydrate (ACS, 99.0-103.0%) and Ammonium hydrogen phosphate (ACS, 98.0% min) were purchased from Alfa Aesar. Ammonium Hydroxide (ACS, 28-30%, BDH CHEMICALS) were used to adjust pH during hydroxyapatite synthesis process. ISOPROPYL ALCOHOL (99%, reagent ACS USP/NF Grade) was bought from PHARMCO-AAPER to form stable hydroxyapatite suspension. Polysulfone (PS, pellets, M_w ~ 35,000 by LS, *SIGMA-ALDRICH*), 1-Methyl-2-Pyrrolidinone (NMP, SEMI Grade, BDH) and Polyvinylpyrrolidone (PVP, MW. av. 40000, TCI) were used as binder, solvent and dispersant respectively in the ceramic suspension. Ethanol (absolute, anhydrous, ACS/USP grade) as internal coagulant was purchased from PHARMCO-AAPER and external coagulant is the tape water. n-Dodecane (99+%, Alfa Aescar) was selected to represent the oil in the oil water emulsion test and sodium dodecyl sulfate (SDS, IDI) was used to form oil water emulsion. All chemicals were used as received without any treatment and Deionized (DI) water was used in all purpose.

4.2.2 Preparation of hydroxyapatite hollow-fiber membranes

Hydroxyapatite powder was synthesized by chemical precipitation. 0.6 M calcium nitrate tetrahydrate and 0.4 M ammonium hydrogen phosphate were slowly mixed together and the mixture was adjusted to pH 10.5 by ammonia hydroxide. The solution was stirred at 80 ^oC for 24hrs and then the precipitate was filtered and washed. Finally, the sample were dried and then calcined at 600 ^oC for 6hrs with air flow. The hydroxyapatite powder was further calcined at 700 ^oC, 800 ^oC, 900 ^oC and 1050 ^oC for 4 hrs by a heating rate of 2 ^oC/min without airflow to discuss the calcination effect on the

hydroxyapatite properties. All hydroxyapatite powder was grinded and sieved through 80 mesh screen before their usage in the preparation of hydroxyapatite hollow fiber.

Hydroxyapatite hollow fiber was prepared by combination of phase inversion method and spinning techniques. A series of hydroxyapatite hollow fiber were prepared from ceramic slurry with varied ratios of NMP, PS, PVP and HAP. For one specific membrane preparation process, PVP and PS were dissolved in the NMP and then HAP was added slowly. The Ceramic slurry was magnetically stirred for 48 hours to homogeneously disperse the particle. The suspension was degassed under vacuum until no bubble emerges. The ceramic slurry was extruded into ceramic hollow fiber precursors through a coaxial spinneret (outer diameter 2.16mm, inner diameter 1.65mm) by a dual drive syringe pump (PMP 33, Harvard apparatus) with the same flow rate (0.5ml/min) of both internal and external coagulant. No air gap existed. Figure 3-11 shows the scheme setup for the hollow up extrusion.

The hollow fiber precursor was left in the water bath overnight to fully complete the phase inversion process. After drying the hollow fiber precursors at room temperature overnight, the green membrane was sintered at 1250 ^{o}C for 4hrs by a Sentro Tech high temperature furnace. The temperature was increased to 600 ^{o}C at 2 ^{o}C/min and held for 4 hours, and then to 1250 ^{o}C at the same heating rate. The sample was cooled down by 5 ^{o}C/min. All the characterizations or tests were measured on the sintered hollow fiber.

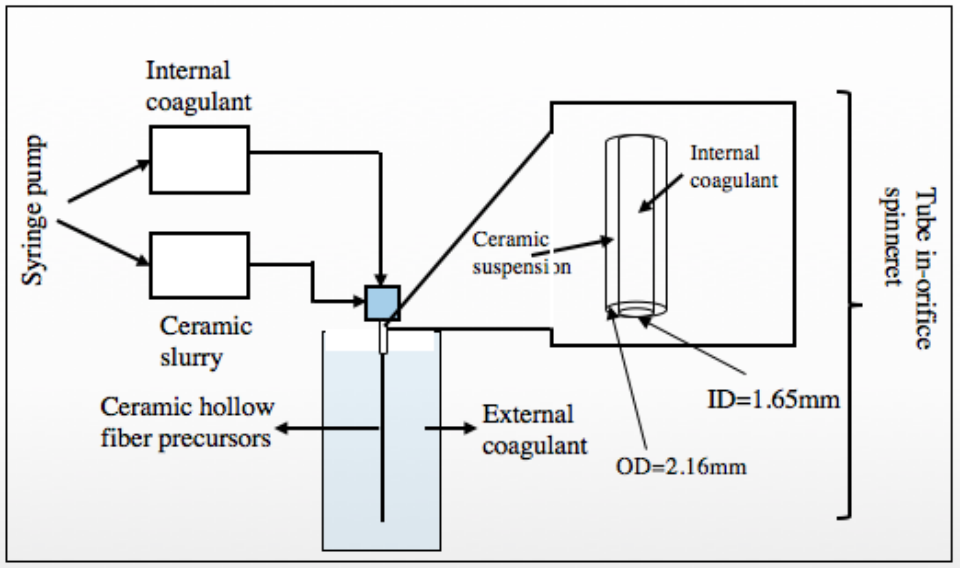

Figure 4-1. Scheme setup for the preparation of ceramic hollow fiber.

4.2.3 Characterization methods

Powder X-ray Diffraction of the synthesized hydroxyapatite were measured by a Bruker D8 Advance Lynx Powder Diffractometer (LynxEye PSD detector, sealed tube, Cu Kα radiation with Ni β-filter). The surface area of the particles was detected by N2 adsorption-desorption isotherms through an Autosorb-iQ analyzer (Quantachrome Instruments). All the samples are degassed at 1mmHg and 245 ^{o}C for 8 hours before measurements. The specific surface area was calculated by Brunauer, Emmett and Teller (BET) method. Dynamic Light Scattering (DLS) was used to measure the particle size of the materials. The measurement was conducted on a Photocor-FC light scattering instrument with a 5-mW laser light source at 633 nm. The measure temperature is 25 ^{o}C and the scattering angle is 90 ^{o}C. The particle sizes could be calculated by the autocorrelation function by the Photocor software and a logarithmic correlator was used to measure the autocorrelation function. For the particle size measurement, since hydroxyapatite particle is unstable in the water, around 0.1 g particles were dissolved in isopropanol and sonicated by Bransonic 1510R-DTH for 30 mins and then diluted 100

times by isopropanol for another 30-min sonication to form stable hydroxyapatite suspension.

The morphologies of hollow fiber membranes were recorded by scanning electron microscopy (SEM) on a Hitachi SU-70 electron microscope. The radial shrinkage ratio was calculated by the length different before and after the sintering. Pore size distribution was measured by mercury intrusion porosimetry on AutoPore IV 9500 V1.07 (Micromeritics Instrument Corporation) between 1.5 psi and 33000 psi with an equilibrium time of 10s, assuming the contact angle of 130 degree and Hg surface tension of 485 dynes/cm. Viscosity measurement was performed by an AR2000 stress controlled rheometer (TA Instruments, Newark, DE) using a 40mm 4' steel cone and plate geometry within the shear rate between10^{-5} and 100 s^{-1} at 25 ^{o}C[86]. The viscosity was measured right after the degas of ceramic suspension and before the spinning process. The bending strength was determined by a four-point binding test setup (Tinius Olsen 10ST) with a 20-mm sample holder (two outer rollers distance L_{out}= 20mm, and two inner rollers distance L_{in}=10mm) and a cross speed of 0.2 mm/min. For each sample, the bending strength was calculated by the following equations:

$$\sigma = \frac{16FKd_{out}}{\pi(d_{out}^4 - d_{in}^4)}$$

where F is the force at fracture for hollow fiber, K is the half distance between inner and outer roller (K= (L_{out}-L_{in})/2), and d_{out} and d_{in} are the outer and inner diameter of the hollow fiber[86]. For each species, four samples were tested and the average represents the bending strength.

4.2.4 Water and oil water emulsion permeation test

DI water and prepared oil water emulsion was fed through membrane to test membrane permeation properties. Oil water emulsion was prepared by addition of 1g SDS, 10ml n-dodecane into 1L DI water. After stirring for two hours, the mixture is stable and turbid emulsion. The size of droplet measure by dynamic light scattering, was in the range of 170nm and 1195nm.

The permeation of water and oil water emulsion through the hydroxyapatite hollow fiber were carried out on a cross flow setup as shown in Figure 2. Dead-end hollow fiber membrane was mounted on a stainless-steel tube by epoxy glue. The driving force for the permeation is the transmembrane pressure or gravity of oil/water mixture. The transmembrane pressure was kept constant as 1 bar for all of tests. The permeated was collected by glass vials and flux could be calculated by the following equations.

$$J = \frac{V}{t \times A \times \Delta P}$$

where J ($L*hr^{-1}m^{-2}bar^{-1}$) is the permeate flux, t is time(hour), A is the outer surface area of hydroxyapatite hollow fiber membrane and ΔP is trans-membrane pressure (bar).

The oil concentration was detected by combination of liquid-liquid extraction and Gas chromatography. 2 ml dichloromethane was added to the permeate each time and the mixture was blended by 100 times up and down to fully transfer the oil into the dichloromethane. Addition of Brine and high speed centrifuge promotes the water and non-water phase separation. The oil concentration was detected by Gas chromatography (Agilent 7693A). The rejection ratio could be calculated by the below equations.

$$Rejection\ ratio\ R = \frac{C_i - C_o}{C_i}$$

where C_i is oil concentration in the feed and C_o is the oil concentration at permeate.

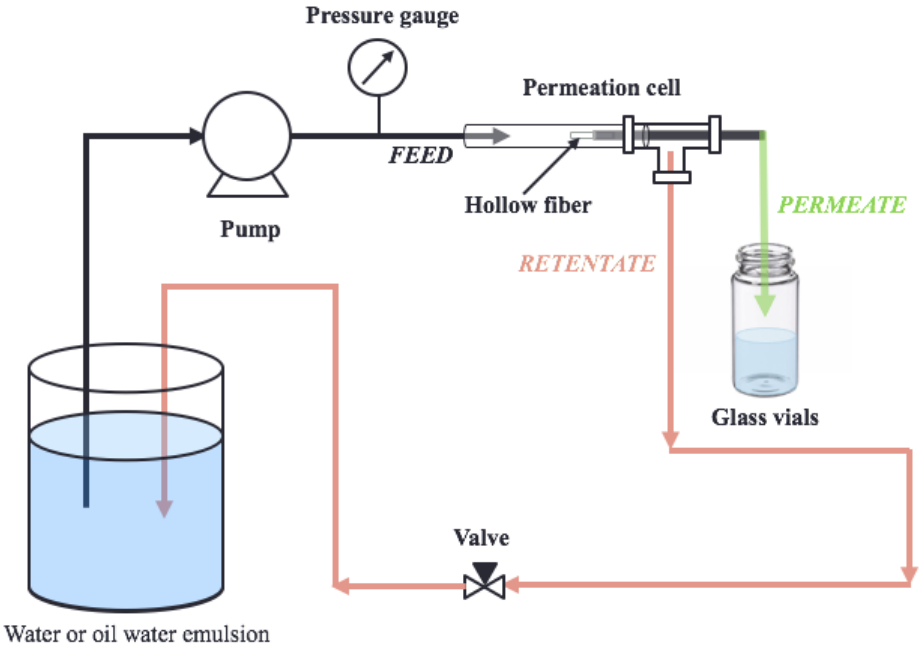

Figure 4-2. Oil water permeation test through a cross flow setup.

4.3 Results and Discussions

4.3.1 Successful Recipes

Recipes of hydroxyapatite hollow fiber prepared with different ceramic suspension are as shown in Table 4-1 to Table 4-4. All hydroxyapatite hollow fibers with uniform and defect free structures were successfully synthesized. Variation of the PS, NMP, organic/inorganic ratio and different particle size was made to discuss their effects on the hydroxyapatite membrane. However, not all of them will be discussed in the following, only hollow fibers from recipe 4, 20 and 15 were characterized and discussed below.

Table 4-1. Four hydroxyapatite hollow fiber recipes with different polysulfone amounts.

Recipe #	PS/wt%	PVP/wt%	NMP/wt%	HAP/wt%	HAP/PS
4	4.41	1.10	50.34	44.13	10
3	5.44	1.08	49.80	43.67	8
2	7.48	1.07	48.74	42.7	5.71
1	7.65	1.09	47.54	43.72	5.72

Table 4-2. Four hydroxyapatite hollow fiber recipes with different N-Methyl-2-pyrrolidone amounts.

Recipe #	NMP/g	PS/wt%	PVP/wt%	NMP/wt%	HAP/wt%	HAP/PS
3	9.1310	5.44	1.08	49.80	43.67	8
5	8.6921	5.62	1.12	48.56	44.70	8
6	11.0223	6.05	1.21	44.35	48.39	8
21	6.7321	6.27	1.25	42.25	50.02	8

Table 4-3. Four hydroxyapatite hollow fiber recipes with different organic/inorganic ratios.

Recipe #	**Organic/inorganic ratio**	**PS/wt%**	**PVP/wt%**	**NMP/wt%**	**HAP/wt%**	**HAP/PS**
3	**1.29**	5.44	1.08	49.80	43.67	8
9	**1.11**	3.17	1.42	48.06	47.34	15
7	**1.09**	1.45	2.84	45.96	47.75	10
8	**1.08**	4.81	1.52	47.09	48.10	10

Table 4-4. Hydroxyapatite hollow fiber recipes with hydroxyapatite power calcined at different temperature

Recipe #	**Calcination temperature(°C)**	**PS/g**	**PVP/g**	**NMP/g**	**HAP/g**	**HAP/PS**
4	**600**	0.7986	0.2001	9.2028	8.0040	10
20	**900**	0.7986	0.2006	7.0474	8.0028	10

30	**1050**	0.8015	0.2016	5.0017	8.0001	10

4.3.2 Morphologies

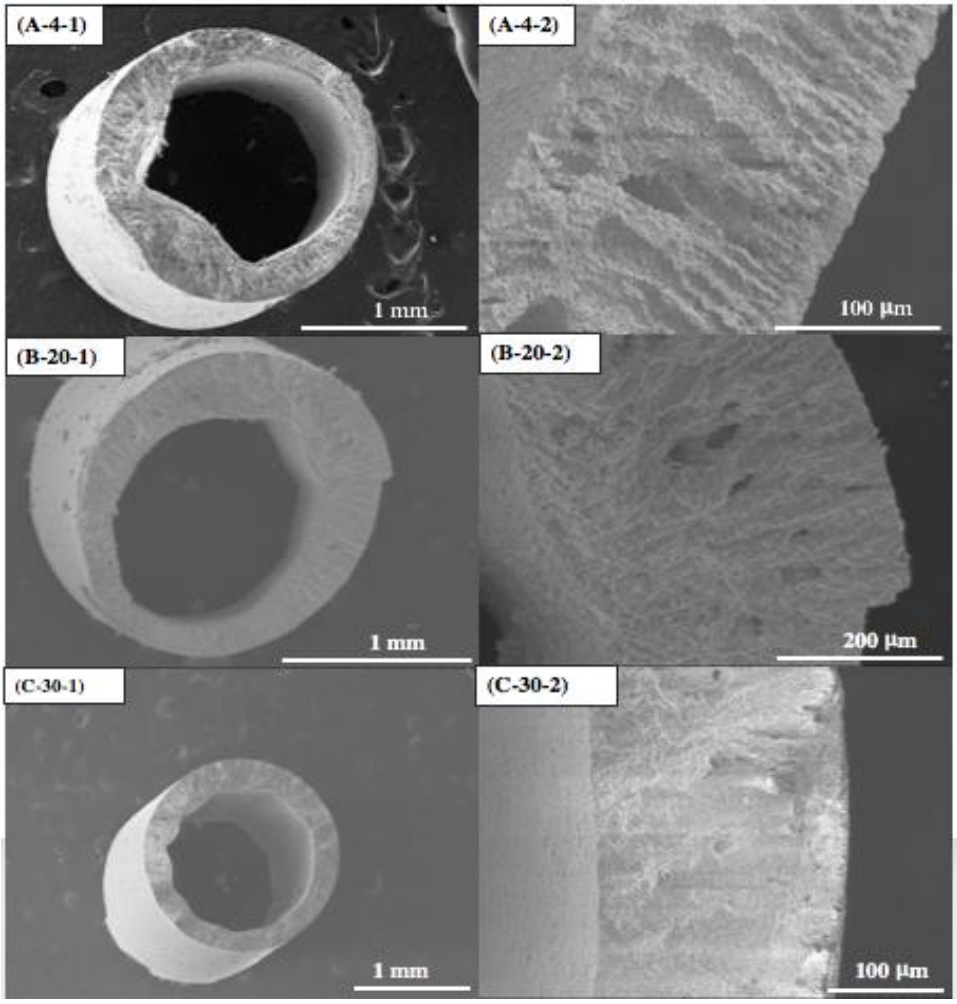

Figure 4-3. Cross section images of hydroxyapatite hollow fiber recipe 4, 20, 30.

The morphologies of hydroxyapatite hollow fiber membrane of recipe 4, 20 and 30 were shown in Figure 4-3. All these three recipes membrane shows a non-symmetric hollow fiber structure with an asymmetric layer structures. For recipe 4 hollow fiber, 5 different layers exist. From outside to inside, they are outside layer, large finger-like layer, sponge layer, small finger-like layer and inside layer. This structure is similar to the Al_2O_3 hollow fiber structure reported before[87]. This sponge-like layer sandwiched by

finger-like layers is the typical structure of the hollow fiber prepared by phase inversion method[88]. During the phase inversion process, the addition of new phase-water disturbs the original stable suspension system and leads to the precipitation of ceramic power and chemical additives. This demixing process formed the hollow fiber structure. The solvent exchange between NMP and coagulant promotes the outbound movement of ceramic particle, in which a relative dense outside layer and macro-void inner layer are formed. During the phase inversion process through a coaxial spinneret, two phase inversion process occurs at the same time. One is between the solvent and external coagulant and the other one is the solvent and internal coagulant. The inner phase inversion process provides the inner finger like structure and the outside phase inversion process forms the outside finger like structure. These two phase inversion processes were contacted and an inner sponge layer formed. In our work, the internal coagulant is ethanol and external coagulant is water. This difference results in the difference in the two finger like structures. Furthermore, the thick inner finger like structure indicates that the phase inversion between ethanol and NMP is weaker than the phase inversion between water and NMP.

Recipe 20 and recipe 30 shows similar sponge layer structures, but only three layers (outside layer, inner layer and one finger like layer) exist as shown in Figure 4-3 B and C. Comparison between recipe 4 and recipe 20 and 30 in Table 4-4 showed the major differences were the particle size and NMP solvent amount. Particle size increased from recipe 4 to recipe 30 and NMP amount decreased. In order to discuss the effect of particle size on the structure of hollow fiber membrane, a group of four hollow fiber membranes

with same recipe (0.2g PVP, 0.8g PS, 8.5g NMP and 8 g HAP) and varied particle sizes are prepared. Table 4-5 shows the properties of these four hollow fiber membranes.

Table 4-5. Properties of hollow fiber membrane recipe 4, 20 and 30.

Recipe #	HAP powder Calcination temperature(°C)	HAP/wt%	Average pore size(nm)	Porosity/%	Shrinkage after sintering (%)
4	600	44.13	633.0	38.95	28.57
20	900	49.86	490.5	40.36	23.59
30	1050	57.14	1576.6	44.78	14.24

As mentioned in chapter 2, variation in calcination temperature results in the changes in particle size. In order to prepare different particle size hydroxyapatite powder, four different calcination temperature from 600 to 900 °C were used to make hydroxyapatite powder with size ranging from 211 to 526 nm. SEM images of these four hollow fiber membranes were shown in Figure 4-4. A similar phenomenon was observed. Hollow fiber A does not show any clear finger like structure and only one sponge layer existed. From hollow fiber B to hollow fiber D, more and more clear finger like structure were observed. In hollow fiber D, five-layer hollow fiber structure was observed. One reasonable explanation for the structure deviation with the particle size is that viscosity changes affect the demix process during the phase inversion process. Rheology properties play a key role in any polymer solution or particle suspensions' shape-forming behavior[89]. High viscous suspension is necessary to prevent the break of continuous fiber into droplets and promote the formation of stable fiber, but too high viscous the ceramic suspension prevents the finger-like void growth[90]. The viscosity of ceramic suspension decreased from hollow fiber A to D. The viscosity of the suspension of hollow fiber A is

4943 Pa.s, which is very high and then totally prevent the particle movement during the phase inversion process. With the decrease of viscosity, the block effect decrease and the finger like structure appeared. The outer surface was porous and B-3 and C-3 had the small pore size than A-3 and C-3. The inner surface showed clear grain boundary and sintering effect. The pore size of inner surface was larger than outer surface.

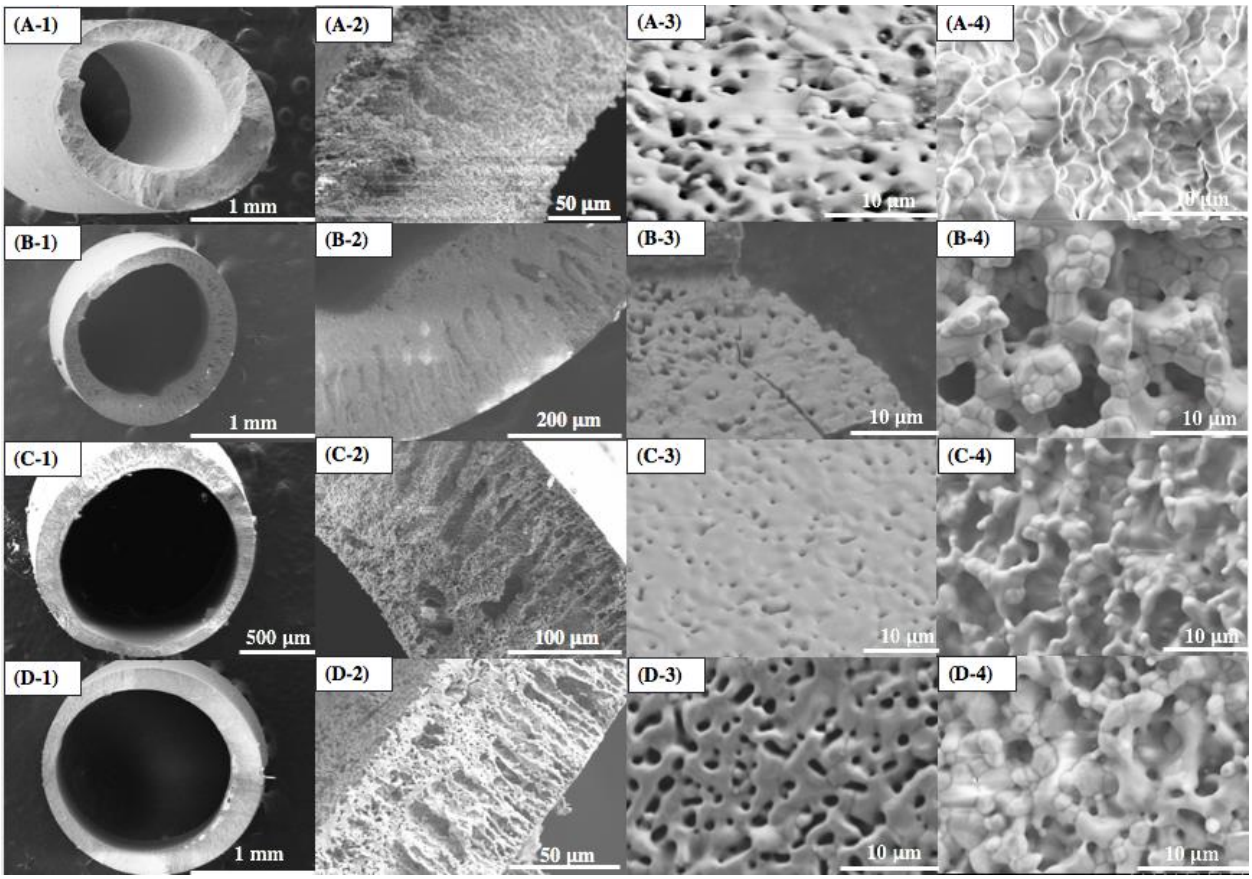

Figure 4-4. SEM images hydroxyapatite hollow fiber membrane prepared with hydroxyapatite power calcined at 600 (A), 700 (B), 800(C) and 900(D) ^{o}C. 3 means the outer layer and 4 means the inner layer.

Table 4-6. Properties of hollow fiber membrane by variation of particle size.

Temperature/^{o}C	Powder size, radius/nm	Viscosity @ 30 1/s (cP)	Shrinkage at 1250 ^{o}C	Bending strength (MPa)	Large pore size(um)	Average pore size (nm)	Porosity (%)
600	211.1696	4943	37.22%	6.35	2.3880	1357.2	29.00
700	231.5163	772.4	29.54%	6.02	0.9132	1541.9	37.33
800	389.6845	923.6	26.78%	4.25	2.9967	1430.3	38.04

900	525.8646	524.2	22.19%	3.29	3.2679	669.1	46.81

The particle size changes also differenced bending strength. Larger particle leads to a smaller bending strength. The relationship between particle size and bending strength satisfies the experienced equation, where tensile strength σ_t is proportional to $1/\sqrt{d_g}$[13]. As shown in the Figure 4-5, the bending strength is proportional to $1/\sqrt{d_g}$ with the R-square equals 99.83%, which means the liner equations fits the data well.

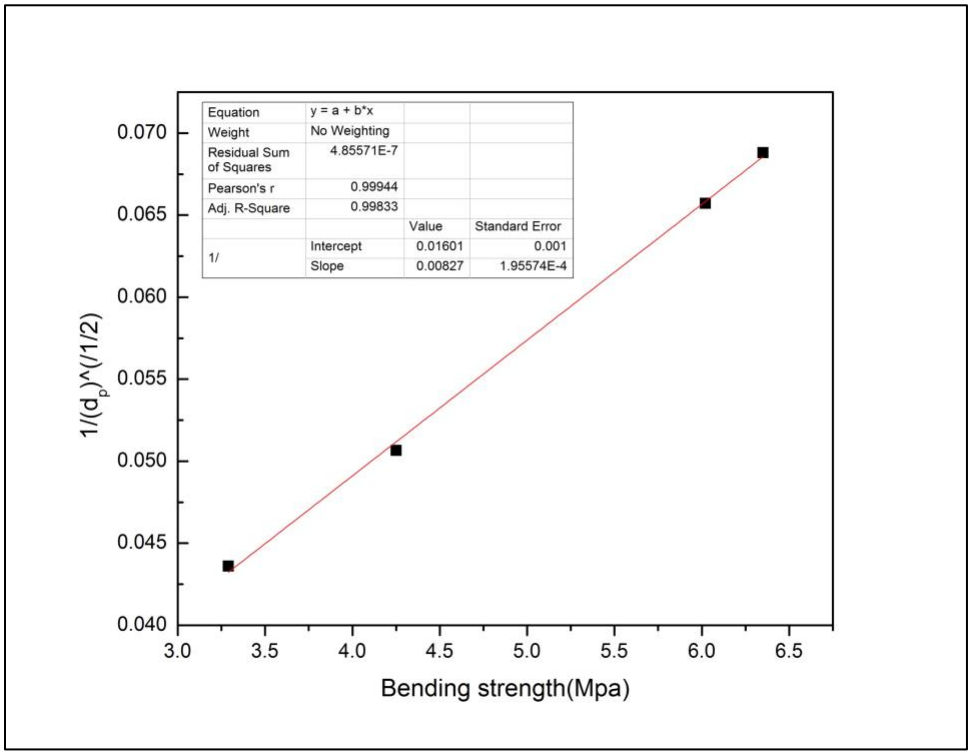

Figure 2-5. The liner relationship between bending strength and $1/\sqrt{d_g}$.

4.3.3 Oil water separations

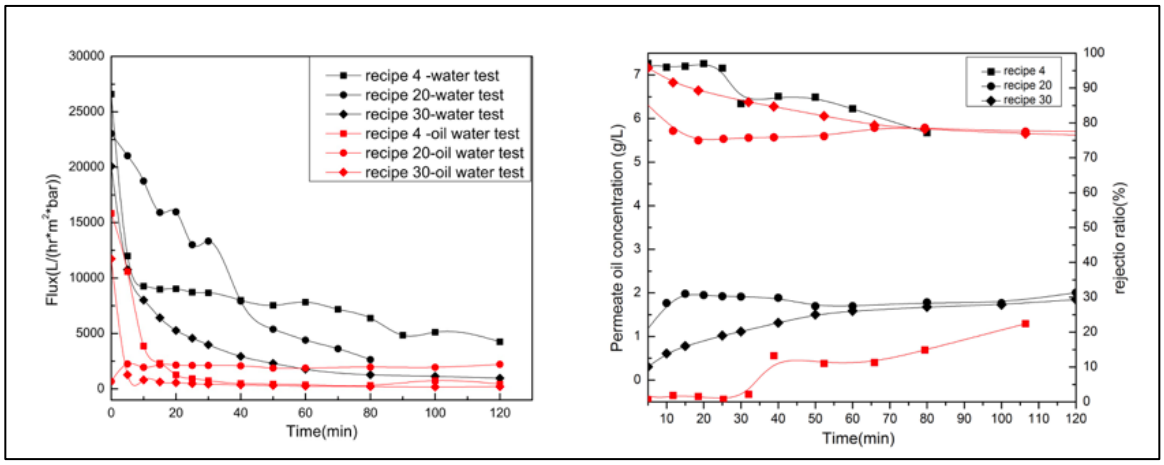

Figure 4-6. Flux(left) and Permeate concentration and rejection ratio (right) of recipe 4, 20 and 30 hydroxyapatites hollow fiber during the water permeation and oil water separation process.

Figure 4-6 shows the water flux, oil water flux, rejection ratio and permeate oil concentration. In the left figure in Figure 4-6, the black means the flux in the water permeation test, and the red equals to the flux in the oily water test. Both flux deceased due to the fouling effect that was caused by the deposition of ions or organics on the pore surface. The flux in the oily water test was lower than the flux in the water test because the fouling effect is more serious in the oily water test and the fact oil droplet size was larger than water molecular size. In the right figure in Figure 4-6, the black lines represent the oil concentration and red lines denote the rejection ratio. Low oil concentration leads to high rejection ratio due to the definition of the rejection ratio. From the rejection ratio variation, recipe 4 membrane barely transport all the mixture and did not inhibit the oil permeation. The separation effect of recipe 20 is better than recipe 4 and recipe 30 shows the best separation effect. More than 90% of the oil was rejected in the beginning and above 75% of the oil could not pass through membrane during the test. These results are not consistent with the average pore size results, which showed that

recipe 30 had the largest average pore size and then the lowest separation effects in respond. Since the hollow fiber have several layers in one membrane, the separation effect is based on the relative dense layer, but the average pore size was calculated according to all the pore size. That explains for the fact that recipe 30 have better separation effect but the average pore size is also the largest.

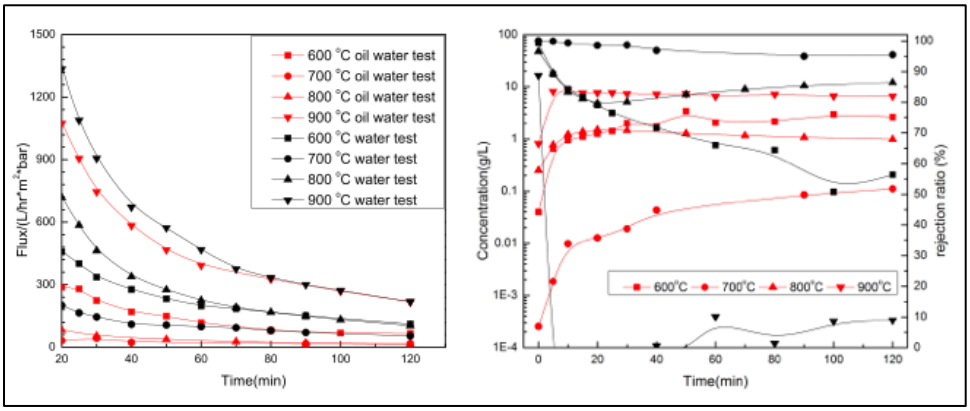

Figure 4-7. Flux(left) and Permeate concentration and rejection ratio (right) of recipe A (600 °C), B (700 °C), C (800 °C) and D (900 °C) hydroxyapatites hollow fiber during the water permeation and oil water separation process.

The flux of water and oily water permeation test was shown in the left figure of Figure 4-7. The water flux was higher than oily water emulsion flux. The fouling effect lead to the flux decrease. The sample 700 °C recipe hollow fiber had the lowest water and oily water flux. The flux is proportional to the pore size, or the pore size of the relative dense layer of the membrane. The pore size distribution was shown in Figure 4-8. For each membrane, two peaks existed. The large one stands for the macrvoid structure and the small one represent the relative dense layer. The 600-recipe sample did not have any macrvoid as shown in the SEM image in Figure 4-4 and the size distribution also proved that. For the relative dense layer pore size in Figure 4-8, the average pore size of 600 and 700 are similar and smaller than 800 and 900 recipe samples. Furthermore, the SEM indicated that the pore size on the outer layer of recipe 600 was larger than recipe 700.

Therefore, recipe 700 had the smallest pore size on the outer layer, which accounted for the lowest flux. Recipe 700 also had good separation results as shown in the right figure in Figure 4-7. More than 95% of the oil was rejected and oil concentration in the beginning was lower than 1mg/L, which satisfied the discharge requirement.

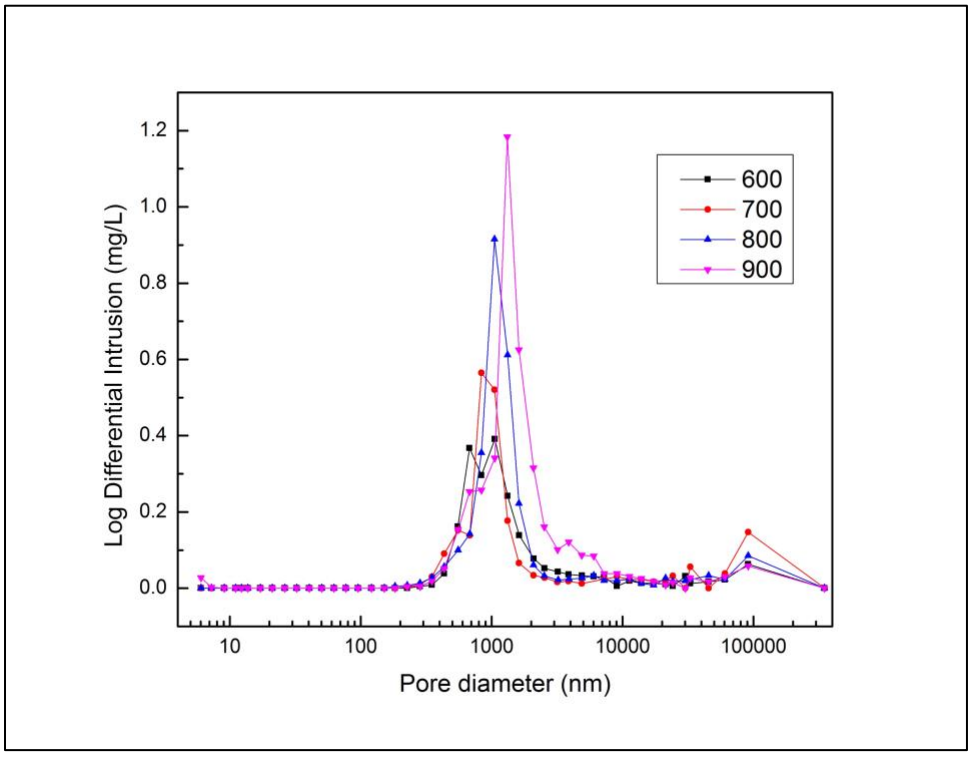

Figure 4-8. Pore size distribution of recipe 600, 700, 800 and 900.

4.3.4 Regeneration of hydroxyapatite hollow fiber membrane

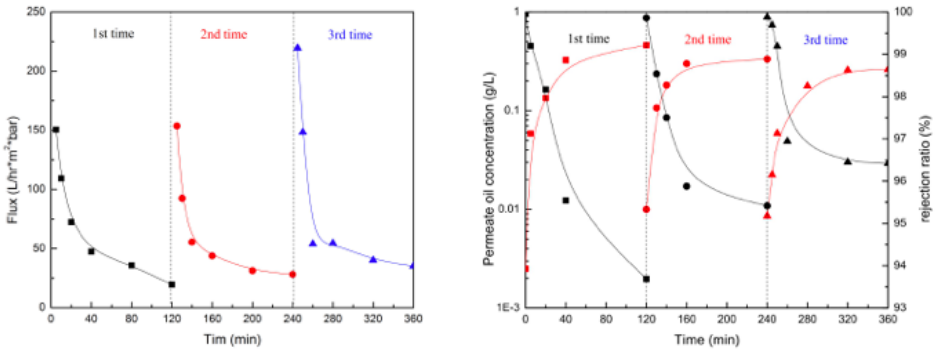

Figure 4-9. (Left) Flux variations of 0-time regeneration (1st time), 1 time regeneration (2nd time) and 2 times regeneration (3rd time); (Right) Permeate oil concentration and rejection ratio of 0-time regeneration (1st time), 1 time regeneration (2nd time) and 2 times regeneration (3rd time).

One unique property of ceramic membrane is its reusability. In this work, used hydroxyapatite hollow fiber membrane was regenerated by calcination in air to remove the source of fouling effect. The oil water permeation results showed that the performance were recovered. As shown in Figure 4-7, the permeate flux decrease due to the fouling effect and initial fluxes are approximately 150 L/(hr*m^2*bar) and the final fluxes are approximately 25 L/(hr*m^2*bar). For the permeate oil concentration and rejection ratio, they also did not change, even though some deviations existed. The slight increase of rejection ratio and decrease of permeate oil concentration are due to incomplete removal of all deposited materials on the pore of membrane. That decreases the pore size and then increases the rejection ratio and decreases the oil concentration.

4.4 Conclusions

A series of hydroxyapatite hollow fiber were successfully synthesized by the phase inversion method through a coaxial spinneret. Particle size is an important factor that determined the morphologies of the membrane. Ceramic suspension needs to be viscous to form the continuous hollow fiber, but when the viscosity of suspension is too high, the solvent exchange during the phase inversion process does not lead to the formation of the finger like macroviod structure. The recipe 700 has the best oil water separation effect due to the relative dense outer layer. More than 95% of the oil was rejected during the test and the oil concentration in the beginning was around 1mg/L, which meets the discharge requirement. The fouling effect during the permeation affected the separation and the oil concentration in the permeate increased. The regeneration ability of the ceramic membrane was also tested by calcination of the used membrane in the air. The flux and oil rejection ability could be recovered after regeneration.

Chapter 5: Coating on hydroxyapatite membrane for the dense membrane.

5.1 Introduction

All the hydroxyapatite hollow fibers synthesized are proved to be porous by water permeation test. Dense hydroxyapatite hollow fibers have potential applications in water permeation and hydrogen permeation due to the existence of the hydroxyl channel[23] and also the proton conductivity[91] of the hydroxyapatite membranes. The prerequisite of these applications is the dense hydroxyapatite membrane. One method to convert porous membrane to dense membrane is coating. There are lots of research and various methods existing to coat a hydroxyapatite layer on another substrate, due to the biocompatibility of hydroxyapatite, such as sol gel and dip coating[92], sputter coating[93], electrochemical deposition[57] and plasma spraying[94]. In this work, considering the substrate is also hydroxyapatite and could act as seeds to grow another hydroxyapatite layer by hydrothermal growth method. For most of the hydroxyapatite coating method, hydroxyapatite is amorphous or poorly crystalline[95]. Additional sintering process is needed to improve the crystallinity since in vivo dissolution of the poorly crystalline HAP films[96]. Hydrothermal growth method has been proved to produced highly crystalline hydroxyapatite[57, 97]. Therefore, hydrothermal growth method is applied to deposit dense hydroxyapatite film on the porous hydroxyapatite hollow fiber. During the common hydrothermal growth process, the mother solutions contains a calcium,

phosphate precursor and the calcium chelating agent such as ethylenediamine tetraacetic acid (EDTA) and lactic acid. The chelating agent promote the supersaturation of HAP and then affect the crystal growth. Following heating supersaturates the solution and then crystal hydroxyapatite forms. In this work, a similar process is performed based on a electrochemical hydrothermal hydroxyapatite coating on Titanium plate[57] to form dense hydroxyapatite layers. In this method, another agent Hexadecltrimethylammonium bromide (CTAB) is added to promote the growth along *a* and *b* axis, otherwise, only *c*-axis hydroxyapatite forms.

5.2 Materials

Calcium Nitrate Tetrahydrate (ACS, 99.0-103.0%), Ammonium hydrogen phosphate (ACS, 98.0% min), Ethylenediaminetetra-acetic acid disodium salt dehydrate (ACS, 99.0-101.0%), (1-Hexadecyl) trimethylammonium bromide (98%, CTAB) were purchased from Alfa Aesar through VWR. Ammonium Hydroxide (ACS, 28-30%) were purchased from BDH CHEMICALS. All chemicals were used as received without any treatment and Deionized (DI) water was used in all purpose.

5.3 Experimental procedure

For a typical hydrothermal growth process, two prepared solutions (solution A and solution B) was mixed and the pH of the mixture was adjusted to 10.0 by ammonia hydroxide. Solution A contains Na_2EDTA (0.20 M), $Ca(NO_3)_2$(0.2M) and 15 ml DI water. 0.12M $(NH_4)_2HPO_4$ was dissolved in solution B (15ml DI water). The mixture was stirred for 20 mins before it was poured into a Teflon-lined stainless steel pressure vessel. Sintered hydroxyapatite hollow fiber was submersed into the solution and then the Teflon vessel was heated up to 200 ^oC for 15 hours. After cooling down, the sample was taken

out and then rinsed by water serval times and dried. One time hydrothermal growth was finished. When the CTAB (0.1M) was needed, the concentration of Na_2EDTA (0.20 M), $Ca(NO_3)_2$(0.2M) and $(NH_4)_2HPO_4$ decreased by half and the other procedures were same. After the hydrothermal growth was finished, the hollow fiber samples were calcined at 700 ^oC for 6 hours with airflow. Three groups hollow fiber membranes were prepared to discuss the coating effects and influence of CTAB. All of three groups undertook four times hydrothermal growth. The first group was prepared without CTAB. In the second group, CTAB was added during only last time hydrothermal growth. The last two hydrothermal growth contains CTAB in the third group.

The morphologies of the membrane were recorded by scanning electron microscopy (SEM) on a Hitachi SU-70 electron microscope.

5.4 Results and Discussions

The SEM images of the group 1 to 3 were shown in Figure 5-1. For all three groups, *c*-axis hydroxyapatite with hexagonal structure could be observed. For the first group (A-0 in Figure 5-1) without CTAB addition, the size of a single hexagonal structure is around 5 **μ**m and some small hydroxyapatite crystals exists due to the deposition of the liquid hydroxyapatite during the hydrothermal growth. The cross section of the hollow fiber shows the thickness of the new layer is around 50 **μ**m. Similar structures also appeared in the second and third group samples (B-1 and C-2). For a single crystal, the size is around 8 and 10 **μ**m in B-1 and C-2 respectively. The width increase is due to the existence of CTAB, which promotes the hydroxyapatite growth in *a* and *b* axis. Furthermore, the existence of CTAB also resulted in crack of the hexagonal structure. That may be due to the different growth rate in different arises. There is no

clear difference in the thickness of the new hydroxyapatite layer for three groups. Furthermore, the new hydroxyapatite layer seems to be dense from the cross view, but gas permeation test is needed to further prove that.

Hydroxyapatite hollow fiber was coated a dense hydroxyapatite layer by hydrothermal growth method using the hollow fiber as seeds.

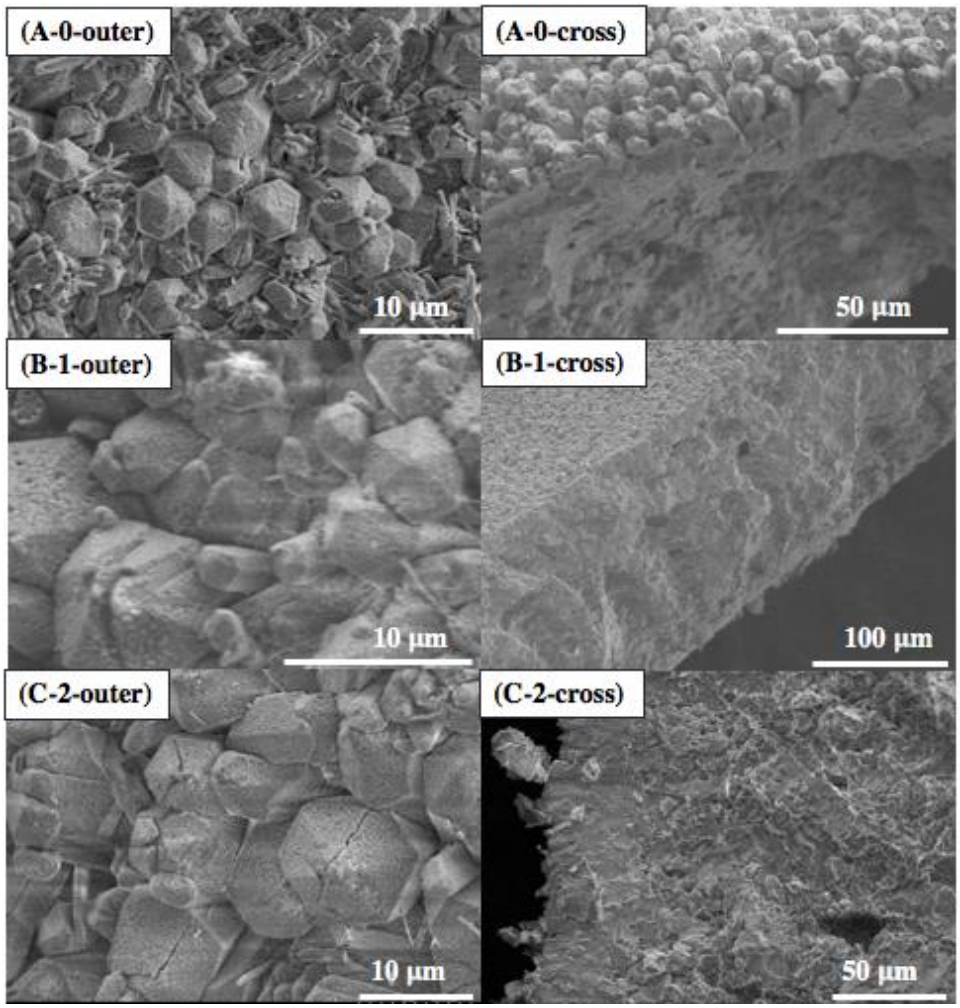

Figure 5-1. SEM images of the outer surface and cross-section of the first group(A-0), second group (B-1) and third group (C-2) hollow fibers.

Chapter 6: Conclusions and Future work

6.1 Conclusions

In this work, different morphologies hydroxyapatite membrane was successfully synthesized by three methods and the application of hydroxyapatite hollow fiber membrane in oil water separation was discussed. Flat and tubular membrane could be synthesized by tape casting method, and the water permeation test and SEM images showed that the membrane is dense. Hydroxyapatite hollow fiber membrane was synthesized by phase inversion method through a single orifice or a coaxial spinneret. The hollow fiber made through a single orifice had a very small diameter but the hollow structure was difficult to form. Hollow fiber was commonly manufactured through a coaxial spinneret and particle size played a key role in determining the morphologies of the membrane by changing the viscosity of the ceramic suspension. A unique hollow fiber showed good oil water separation efficiency by rejecting 95% of the oil and regeneration ability by fully recovery of the flux and rejection ratio. The particle size also influence the bending strength of the membrane and the relationship between them satisfied an experienced equation. This is the first work that hydroxyapatite hollow fiber was synthesized and HAP hollow fiber showed great potential in oil water separation.

6.2 Future work

6.2.1 Internal coagulant influence on the structure of hollow fiber

During the manufacture of the hollow fiber membrane, two phase inversion processes exist. One is between the external coagulant and suspension solution, and the other one is between the internal coagulant and suspension solution. The external coagulant is mostly water, but the internal coagulant varies. Different internal coagulants lead to varied internal phase inversion, which leads to the inner layer structure of the hollow fiber membrane. Small phase inversion process avoids the second void layer close to the lumen. Equal phase inversion process between the internal and external leads to symmetric hollow fiber with fiver layers. From outside to inside, the layers are the relative dense thin outside layer, the out void layer, a sponge layer, the inner void layer and a thin inner layer. Therefore, variation in the internal coagulant (such as water, ethanol, 50%wt solvent and water) produces different structure hollow fibers. Experiments by variation of internal coagulant and morphologies recorded by SEM could prove this effect.

6.2.2 Sintering conditions on the structure of hydroxyapatite hollow fiber

Hydroxyapatite decomposes during the sintering process, since the sintering temperature is higher than the dehydration temperature of the hydroxyapatite. Small part of hydroxyapatite convert to TCP, which leads to impurities in the hydroxyapatite hollow fiber membrane. Several methods exist to prevent the decomposition of the hydroxyapatite hollow fiber, such as flow of steam during the sintering process could inhibit this process. Furthermore, diverse sintering temperature results in different sintering effects and the sintering temperature that leads to dense top hollow fiber layer is

still unknown. Therefore, the sintering condition is another topic that is in need to discuss about in the future.

6.2.3 Dense hollow fiber coated by hydrothermal growth

Dense hydroxyapatite hollow fiber has potential applications in hydrogen and water permeation. However, due to the decomposing of hydroxyapatite at high temperature, it is difficult to make dense hydroxyapatite hollow fiber membrane through sintering method. A simple way to make dense hydroxyapatite is coating a dense layer on the top layer. In chapter 5, addition hydroxyapatite layer was successfully added by hydrothermal growth, but no experiments were done to prove it. Therefore, gas permeation test on these coated hydroxyapatite hollow fibers is in need to prove the dense properties of the membrane.

Reference

1. Syarifah Nazirah, W. I.; Yusof, N.; Farhana, A.; Nurasyikin, M., A review of oilfield wastewater treatment using membrane filtration over conventional technology. 2017; p 643-658.
2. Fakhru'l-Razi, A.; Pendashteh, A.; Abdullah, L. C.; Biak, D. R. A.; Madaeni, S. S.; Abidin, Z. Z., Review of technologies for oil and gas produced water treatment. **2009,** 170 (2), 530-551.
3. Baker, R. W., Research needs in the membrane separation industry: Looking back, looking forward. **2010,** 362 (1), 134-136.
4. Neff, J. M., Bioaccumulation in Marine Organisms: Effect of Contaminants from Oil Well Produced Water. Elsevier Science: 2002.
5. Chen, X.; Hong, L.; Xu, Y.; Ong, Z. W., Ceramic Pore Channels with Inducted Carbon Nanotubes for Removing Oil from Water. ACS Applied Materials & Interfaces **2012,** 4 (4), 1909-1918.
6. Padaki, M.; Surya Murali, R.; Abdullah, M. S.; Misdan, N.; Moslehyani, A.; Kassim, M. A.; Hilal, N.; Ismail, A. F., Membrane technology enhancement in oil–water separation. A review. **2015,** 357, 197-207.
7. Basile, A.; Gallucci, F., Membranes for Membrane Reactors: Preparation, Optimization and Selection. Wiley: 2010.
8. Liu, D.-M., Porous Ceramic Materials: Fabrication, Characterization, Applications. Trans Tech Publications: 1996.
9. Koros, W. J.; Ma, Y. H.; Shimidzu, T., Terminology for membranes and membrane processes (IUPAC Recommendations 1996). In Pure and Applied Chemistry, 1996; Vol. 68, p 1479.
10. Strathmann, H., Introduction to Membrane Science and Technology. Wiley: 2011.
11. Nunes, S. P.; Peinemann, K. V., Membrane Technology: in the Chemical Industry. Wiley: 2006.
12. The Basics. In Ceramic Membranes: New Opportunities and Practical Applications, Wiley-VCH Verlag GmbH & Co. KGaA: 2016; pp 1-90.
13. Maarten Biesheuvel, P.; Verweij, H., Design of ceramic membrane supports: permeability, tensile strength and stress. **1999,** 156 (1), 141-152.
14. Bhave, R., Inorganic Membranes Synthesis, Characteristics and Applications: Synthesis, characteristics, and applications. Springer Netherlands: 2012.
15. Aste, T., Variations around disordered close packing. Journal of Physics: Condensed Matter **2005,** 17 (24), S2361.
16. Onoda, G. Y.; Hench, L. L.; Florida, U. o., Ceramic processing before firing. Wiley: 1978.
17. Li, K., Ceramic Membranes and Membrane Processes.
18. Li, K., Preparation of Ceramic Membranes. In Ceramic Membranes for Separation and Reaction, John Wiley & Sons, Ltd: 2007; pp 21-57.
19. Ebrahimi, M.; Willershausen, D.; Ashaghi, K. S.; Engel, L.; Placido, L.; Mund, P.; Bolduan, P.; Czermak, P., Investigations on the use of different ceramic membranes for efficient oil-field produced water treatment. **2010,** 250 (3), 991-996.

20. Zhang, L. J.; Webster, T. J., Nanotechnology and nanomaterials: Promises for improved tissue regeneration. Nano Today **2009,** 4 (1), 66-80.
21. Hughes, J. M., Structure and Chemistry of the Apatites and Other Calcium Orthophosphates By J. C. Elliot (The London Hospital Medical College). Elsevier: Amsterdam. 1994. xii + 389 pp. ISBN 0-444-81582-1. Journal of the American Chemical Society **1996,** 118 (12), 3072-3072.
22. Cao, H.; Zhang, L.; Zheng, H.; Wang, Z., Hydroxyapatite Nanocrystals for Biomedical Applications. The Journal of Physical Chemistry C **2010,** 114 (43), 18352-18357.
23. Uskoković, V., The Role of Hydroxyl Channel in Defining Selected Physicochemical Peculiarities Exhibited by Hydroxyapatite. RSC advances **2015,** 5, 36614-36633.
24. Rivera-Munoz, E. M., Hydroxyapatite-Based Materials: Synthesis and Characterization. In Biomedical Engineering - Frontiers and Challenges, FazelRezai, R., Ed. Intech Europe: Rijeka, 2011; pp 75-98.
25. Okada, M.; Matsumoto, T., Synthesis and modification of apatite nanoparticles for use in dental and medical applications. **2015,** 51 (4), 85-95.
26. Muralithran, G.; Ramesh, S., The effects of sintering temperature on the properties of hydroxyapatite. **2000,** 26 (2), 221-230.
27. FULMER, M. T.; BROWN, P. W., Hydrolysis of dicalcium phosphate dihydrate to hydroxyapatite. Journal of Materials Science: Materials in Medicine **1998,** 9 (4), 197-202.
28. Uskoković, V.; Uskoković Dragan, P., Nanosized hydroxyapatite and other calcium phosphates: Chemistry of formation and application as drug and gene delivery agents. Journal of Biomedical Materials Research Part B: Applied Biomaterials **2010,** 96B (1), 152-191.
29. Sadat-Shojai, M.; Khorasani, M.-T.; Dinpanah-Khoshdargi, E.; Jamshidi, A., Synthesis methods for nanosized hydroxyapatite with diverse structures. **2013,** 9 (8), 7591-7621.
30. Tsuchida, T.; Kubo, J.; Yoshioka, T.; Sakuma, S.; Takeguchi, T.; Ueda, W., Reaction of ethanol over hydroxyapatite affected by Ca/P ratio of catalyst. Journal of Catalysis **2008,** 259 (2), 183-189.
31. Sebti, S. d.; Tahir, R.; Nazih, R.; Boulaajaj, S. d., Comparison of different Lewis acid supported on hydroxyapatite as new catalysts of Friedel–Crafts alkylation. **2001,** 218 (1), 25-30.
32. Kibby, C. L.; Hall, W. K., Dehydrogenation of alcohols and hydrogen transfer from alcohols to ketones over hydroxyapatite catalysts. **1973,** 31 (1), 65-73.
33. Lin, K.; Pan, J.; Chen, Y.; Cheng, R.; Xu, X., Study the adsorption of phenol from aqueous solution on hydroxyapatite nanopowders. **2009,** 161 (1), 231-240.
34. Hashimoto, Y.; Taki, T.; Sato, T., Sorption of dissolved lead from shooting range soils using hydroxyapatite amendments synthesized from industrial byproducts as affected by varying pH conditions. **2009,** 90 (5), 1782-1789.
35. Bouhaouss, A.; Bensaoud, A.; Laghzizil, A.; Ferhat, M., Effect of chemical treatments on the ionic conductivity of carbonate apatite. **2001,** 3 (6), 437-441.

36. Mahabole, M. P.; Aiyer, R. C.; Ramakrishna, C. V.; Sreedhar, B.; Khairnar, R. S., Synthesis, characterization and gas sensing property of hydroxyapatite ceramic. **2005,** 28 (6), 535-545.
37. Cummings, L. J.; Snyder, M. A.; Brisack, K.; Burgess, R. R.; Deutscher, M. P., Chapter 24 Protein Chromatography on Hydroxyapatite Columns. In Guide to Protein Purification, 2nd Edition, Academic Press: 2009; Vol. 463, pp 387-404.
38. Teshima, K.; Lee, S.; Sakurai, M.; Kameno, Y.; Yubuta, K.; Suzuki, T.; Shishido, T.; Endo, M.; Oishi, S., Well-Formed One-Dimensional Hydroxyapatite Crystals Grown by an Environmentally Friendly Flux Method. Crystal Growth & Design **2009,** 9 (6), 2937-2940.
39. Pramanik, S.; Agarwal, A. K.; Rai, K. N.; Garg, A., Development of high strength hydroxyapatite by solid-state-sintering process. Ceramics International **2007,** 33 (3), 419-426.
40. Guo, X. J.; Yan, H. D.; Zhao, S. G.; Zhang, L.; Li, Y. T.; Liang, X. H., Effect of calcining temperature on particle size of hydroxyapatite synthesized by solid-state reaction at room temperature. Advanced Powder Technology **2013,** 24 (6), 1034-1038.
41. Mochales, C.; Wilson, R. M.; Dowker, S. E. P.; Ginebra, M. P., Dry mechanosynthesis of nanocrystalline calcium deficient hydroxyapatite: Structural characterisation. Journal of Alloys and Compounds **2011,** 509 (27), 7389-7394.
42. Fathi, M. H.; Zahrani, E. M., Mechanochemical synthesis of fluoridated hydroxyapatite nanopowder. International Journal of Modern Physics B **2008,** 22 (18-19), 3099-3106.
43. Kim, W.; Zhang, Q. W.; Saito, F., Mechanochemical synthesis of hydroxyapatite from Ca(OH)(2)-P2O5 and CaO-Ca(OH)(2)-P2O5 mixtures. Journal of Materials Science **2000,** 35 (21), 5401-5405.
44. Wei, G.; Reichert, J.; Bossert, J.; Jandt, K. D., Novel Biopolymeric Template for the Nucleation and Growth of Hydroxyapatite Crystals Based on Self-Assembled Fibrinogen Fibrils. Biomacromolecules **2008,** 9 (11), 3258-3267.
45. Verwilghen, C.; Chkir, M.; Rio, S.; Nzihou, A.; Sharrock, P.; Depelsenaire, G., Convenient conversion of calcium carbonate to hydroxyapatite at ambient pressure. Materials Science & Engineering C-Biomimetic and Supramolecular Systems **2009,** 29 (3), 771-773.
46. Shanthi, P. M. S.; Ashok, M.; Balasubramanian, T.; Riyasdeen, A.; Akbarsha, M. A., Synthesis and characterization of nano-hydroxyapatite at ambient temperature using cationic surfactant. Materials Letters **2009,** 63 (24-25), 2123-2125.
47. Wang, P. P.; Li, C. H.; Gong, H. Y.; Jiang, X. R.; Wang, H. Q.; Li, K. X., Effects of synthesis conditions on the morphology of hydroxyapatite nanoparticles produced by wet chemical process. Powder Technology **2010,** 203 (2), 315-321.
48. Kim, D. W.; Cho, I. S.; Kim, J. Y.; Jang, H. L.; Han, G. S.; Ryu, H. S.; Shin, H.; Jung, H. S.; Kim, H.; Hong, K. S., Simple Large-Scale Synthesis of Hydroxyapatite Nanoparticles: In Situ Observation of Crystallization Process. Langmuir **2010,** 26 (1), 384-388.
49. Montazeri, N.; Jahandideh, R.; Biazar, E., Synthesis of fluorapatite-hydroxyapatite nanoparticles and toxicity investigations. International Journal of Nanomedicine **2011,** 6, 197-201.

50. Sanosh, K. P.; Chu, M. C.; Balakrishnan, A.; Kim, T. N.; Cho, S. J., Preparation and characterization of nano-hydroxyapatite powder using sol-gel technique. Bulletin of Materials Science **2009,** 32 (5), 465-470.
51. Milev, A.; Kannangara, G. S. K.; Ben-Nissan, B., Morphological stability of hydroxyapatite precursor. Materials Letters **2003,** 57 (13-14), 1960-1965.
52. Ponomareva, N. I.; Poprygina, T. D.; Karpov, S. I.; Lesovoi, M. V.; Agapov, B. L., Microemulsion method for producing hydroxyapatite. Russian Journal of General Chemistry **2010,** 80 (5), 905-908.
53. Chen, B. H.; Chen, K. I.; Ho, M. L.; Chen, H. N.; Chen, W. C.; Wang, C. K., Synthesis of calcium phosphates and porous hydroxyapatite beads prepared by emulsion method. Materials Chemistry and Physics **2009,** 113 (1), 365-371.
54. Furuzono, T.; Walsh, D.; Sato, K.; Sonoda, K.; Tanaka, J., Effect of reaction temperature on the morphology and size of hydroxyapatite nanoparticles in an emulsion system. Journal of Materials Science Letters **2001,** 20 (2), 111-114.
55. Monma, H.; Kamiya, T., Preparation of hydroxyapatite by the hydrolysis of brushite. Journal of Materials Science **1987,** 22 (12), 4247-4250.
56. Park, H. C.; Baek, D. J.; Park, Y. M.; Yoon, S. Y.; Stevens, R., Thermal stability of hydroxyapatite whiskers derived from the hydrolysis of α-TCP. Journal of Materials Science **2004,** 39 (7), 2531-2534.
57. Liu, D.; Savino, K.; Yates, M. Z., Coating of hydroxyapatite films on metal substrates by seeded hydrothermal deposition. **2011,** 205 (16), 3975-3986.
58. Zhou, Z.-H.; Zhou, P.-L.; Yang, S.-P.; Yu, X.-B.; Yang, L.-Z., Controllable synthesis of hydroxyapatite nanocrystals via a dendrimer-assisted hydrothermal process. **2007,** 42 (9), 1611-1618.
59. Loo, S. C. J.; Siew, Y. E.; Ho, S.; Boey, F. Y. C.; Ma, J., Synthesis and hydrothermal treatment of nanostructured hydroxyapatite of controllable sizes. Journal of Materials Science: Materials in Medicine **2008,** 19 (3), 1389-1397.
60. Rameshbabu, N.; Rao, K. P.; Kumar, T. S. S., Acclerated microwave processing of nanocrystalline hydroxyapatite. Journal of Materials Science **2005,** 40 (23), 6319-6323.
61. Wang, Y.-Z.; Fu, Y., Microwave-hydrothermal synthesis and characterization of hydroxyapatite nanocrystallites. **2011,** 65 (23), 3388-3390.
62. Teoreanu, I.; Preda, M.; Melinescu, A., Synthesis and characterization of hydroxyapatite by microwave heating using CaSO4·2H2O and Ca(OH)2 as calcium source. Journal of Materials Science: Materials in Medicine **2008,** 19 (2), 517-523.
63. Hongquan, Z.; Yuhua, Y.; Youfa, W.; Shipu, L., Morphology and formation mechanism of hydroxyapatite whiskers from moderately acid solution. Materials Research **2003,** 6, 111-115.
64. Koutsopoulos, S.; Barlos, K.; Gatos, D.; Dalas, E., The effect of various Prothymosin α fragments on the crystal growth of hydroxyapatite in aqueous solution. **2004,** 267 (1), 306-311.
65. Bucholz, R. W.; Carlton, A.; Holmes, R., Interporous hydroxyapatite as a bone graft substitute in tibial plateau fractures. Clin Orthop Relat Res **1989,** (240), 53-62.
66. Karabulut, A.; Bastan, F. E.; Erdogan, G.; Ustel, F. In Heat Treatment's Effects on Hydroxyapatite Powders in Water Vapor and Air Atmosphere, 4th International Congress

in Advances in Applied Physics and Materials Science (APMAS), Fethiye, TURKEY, Apr 24-27; Amer Inst Physics: Fethiye, TURKEY, 2014.
67. Cullity, B. D.; Stock, S. R., Elements of x-ray diffraction. Prentice Hall: Upper Saddle River, NJ :, 2001.
68. Grader, G. S.; Zuri, L., Tape Casting Slip Preparation by in Situ Polymerization. **1993,** 76 (7), 1809-1814.
69. Jabbari, M.; Bulatova, R.; Tok, A. I. Y.; Bahl, C. R. H.; Mitsoulis, E.; Hattel, J. H., Ceramic tape casting: A review of current methods and trends with emphasis on rheological behaviour and flow analysis. Materials Science and Engineering B-Advanced Functional Solid-State Materials **2016,** 212, 39-61.
70. Young, A. C.; Jane-Chyi, L.; Tsung-Shou, Y.; Chian-Lii, C., Characteristics of tape casting slurries containing forsterite, PVB and organic solvent. **1993,** 34 (2), 147-153.
71. Athayde, D. D.; Souza, D. F.; Silva, A. M. A.; Vasconcelos, D.; Nunes, E. H. M.; Diniz da Costa, J. C.; Vasconcelos, W. L., Review of perovskite ceramic synthesis and membrane preparation methods. **2016,** 42 (6), 6555-6571.
72. Zhang, Y.; Qin, C.; Binner, J., Processing multi-channel alumina membranes by tape casting latex-based suspensions. 2006.
73. Organic Additives and Ceramic Processing With Applications in Powder Metallurgy, Ink, and Paint. Springer Verlag: 2013.
74. Onoda, G. Y., Theoretical Strength of Dried Green Bodies with Organic Binders. **1976,** 59 (5-6), 236-239.
75. Hutchison, R. B.; Curry-Hyde, H. E.; Raper, J. A., Preparation of composite ceramic membrane from titania powders. **1994,** 81 (3), 249-257.
76. Lin, B.; Zhang, S.; Zhang, L.; Bi, L.; Ding, H.; Liu, X.; Gao, J.; Meng, G., Prontonic ceramic membrane fuel cells with layered GdBaCo2O5+x cathode prepared by gel-casting and suspension spray. **2008,** 177 (2), 330-333.
77. Zhang, X.; Wang, D. K.; Lopez, D. R. S.; Diniz da Costa, J. C., Fabrication of nanostructured TiO2 hollow fiber photocatalytic membrane and application for wastewater treatment. **2014,** 236, 314-322.
78. Tan, X.; Li, K., Fundamentals of Membrane Reactors. In Inorganic Membrane Reactors, John Wiley & Sons, Ltd: 2014; pp 1-26.
79. Porter, M. C., Handbook of Industrial Membrane Technology. Noyes Publications: 1990.
80. Mulder, M., Basic principles of membrane technology. Kluwer Acad. Publ.: Dordrecht, 2010.
81. Peng, N.; Widjojo, N.; Sukitpaneenit, P.; Teoh, M. M.; Lipscomb, G. G.; Chung, T.-S.; Lai, J.-Y., Evolution of polymeric hollow fibers as sustainable technologies: Past, present, and future. Topical Issue on Polymer Physics **2012,** 37 (10), 1401-1424.
82. Yao, J.; Wang, K.; Ren, M.; Zhe Liu, J.; Wang, H., Phase inversion spinning of ultrafine hollow fiber membranes through a single orifice spinneret. **2012,** 421-422, 8-14.
83. van de Witte, P.; Dijkstra, P. J.; van den Berg, J. W. A.; Feijen, J., Phase separation processes in polymer solutions in relation to membrane formation. **1996,** 117 (1), 1-31.

84. Chen, P.-C.; Xu, Z.-K., Mineral-Coated Polymer Membranes with Superhydrophilicity and Underwater Superoleophobicity for Effective Oil/Water Separation. **2013,** 3, 2776.
85. McNaught, A. D.; Wilkinson, A.; Chemistry, I. U. o. P. a. A., Compendium of Chemical Terminology: IUPAC Recommendations. Blackwell Science: 1997.
86. de Wit, P.; van Daalen, F. S.; Benes, N. E., The mechanical strength of a ceramic porous hollow fiber. **2017,** 524, 721-728.
87. Koonaphapdeelert, S.; Li, K., Preparation and characterization of hydrophobic ceramic hollow fibre membrane. **2007,** 291 (1), 70-76.
88. Tan, X.; Liu, S.; Li, K., Preparation and characterization of inorganic hollow fiber membranes. **2001,** 188 (1), 87-95.
89. Bergström, L., Rheological Properties of Concentrated, Nonaqueous Silicon Nitride Suspensions. Journal of the American Ceramic Society **2005,** 79 (12), 3033-3040.
90. Kingsbury, B. F. K.; Li, K., A morphological study of ceramic hollow fibre membranes. **2009,** 328 (1), 134-140.
91. Nagai, M.; Shibuya, Y.; Nishino, T.; Saeki, T.; Owada, H.; Yamashita, K.; Umegaki, T., Electrical conductivity of calcium phosphate ceramics with various Ca/P ratios. **1991,** 26 (11), 2949-2953.
92. García, C.; Ceré, S.; Durán, A., Bioactive coatings prepared by sol–gel on stainless steel 316L. Proceedings of the 6th Brazilian Symposium of Glases and Related Materials and 2nd International Symposium on Non-Crystalline Solids in Brazil **2004,** 348, 218-224.
93. Yang, Y.; Kim, K.-H.; Ong, J. L., A review on calcium phosphate coatings produced using a sputtering process—an alternative to plasma spraying. **2005,** 26 (3), 327-337.
94. Chu, P. K.; Chen, J. Y.; Wang, L. P.; Huang, N., Plasma-surface modification of biomaterials. **2002,** 36 (5), 143-206.
95. Roome, C. M.; Adam, C. D., Crystallite orientation and anisotropic strains in thermally sprayed hydroxyapatite coatings. **1995,** 16 (9), 691-696.
96. Xue, W.; Tao, S.; Liu, X.; Zheng, X.; Ding, C., In vivo evaluation of plasma sprayed hydroxyapatite coatings having different crystallinity. **2004,** 25 (3), 415-421.
97. Mengeot, M.; Harvill, M. L.; Gilliam, O. R., Hydrothermal growth of calcium hydroxyapatite single crystals. **1973,** 19 (3), 199-203.